CRISPR/Cas9 Engineering of Adult Mouse Liver Demonstrates That the Dnajb1–Prkaca Gene Fusion Is Sufficient to Induce Tumors Resembling Fibrolamellar Hepatocellular Carcinoma

Engelholm, Lars H.; Riaz, Anjum; Serra, Denise; Dagnæs-Hansen, Frederik; Johansen, Jens V.; Santoni-Rugiu, Eric; Hansen, Steen H.; Niola, Francesco; Frödin, Morten

Published in:
Gastroenterology

DOI:
10.1053/j.gastro.2017.09.008

Publication date:
2017

Document version
Publisher's PDF, also known as Version of record

Gastroenterology 2017;153:1662–1673

CRISPR/Cas9 Engineering of Adult Mouse Liver Demonstrates That the *Dnajb1–Prkaca* Gene Fusion Is Sufficient to Induce Tumors Resembling Fibrolamellar Hepatocellular Carcinoma

Lars H. Engelholm,[1,2] Anjum Riaz,[2] Denise Serra,[2] Frederik Dagnæs-Hansen,[3] Jens V. Johansen,[2] Eric Santoni-Rugiu,[4] Steen H. Hansen,[2,5] Francesco Niola,[2,§] and Morten Frödin[2,§]

[1]*Finsen Laboratory, Rigshospitalet, Copenhagen, Denmark;* [2]*Biotech Research and Innovation Centre, Faculty of Health and Medical Sciences, University of Copenhagen, Copenhagen, Denmark;* [3]*Department of Biomedicine, Aarhus University, Aarhus C, Denmark;* [4]*Department of Pathology, Rigshospitalet, Copenhagen University Hospital, Copenhagen, Denmark;* [5]*GI Cell Biology Research Laboratory, Boston Children's Hospital and Harvard Medical School, Boston, Massachusetts*

BACKGROUND & AIMS: Fibrolamellar hepatocellular carcinoma (FL-HCC) is a primary liver cancer that predominantly affects children and young adults with no underlying liver disease. A somatic, 400 Kb deletion on chromosome 19 that fuses part of the DnaJ heat shock protein family (Hsp40) member B1 gene (*DNAJB1*) to the protein kinase cAMP-activated catalytic subunit alpha gene (*PRKACA*) has been repeatedly identified in patients with FL-HCC. However, the *DNAJB1–PRKACA* gene fusion has not been shown to induce liver tumorigenesis. We used the CRISPR/Cas9 technique to delete in mice the syntenic region on chromosome 8 to create a *Dnajb1–Prkaca* fusion and monitored the mice for liver tumor development. **METHODS:** We delivered CRISPR/Cas9 vectors designed to juxtapose exon 1 of *Dnajb1* with exon 2 of *Prkaca* to create the *Dnajb1–Prkaca* gene fusion associated with FL-HCC, or control Cas9 vector, via hydrodynamic tail vein injection to livers of 8-week-old female FVB/N mice. These mice did not have any other engineered genetic alterations and were not exposed to liver toxins or carcinogens. Liver tissues were collected 14 months after delivery; genomic DNA was analyzed by PCR to detect the *Dnajb1–Prkaca* fusion, and tissues were characterized by histology, immunohistochemistry, RNA sequencing, and whole-exome sequencing. **RESULTS:** Livers from 12 of the 15 mice given the vectors to induce the *Dnajb1–Prkaca* gene fusion, but none of the 11 mice given the control vector, developed neoplasms. The tumors contained the *Dnajb1–Prkaca* gene fusion and had histologic and cytologic features of human FL-HCCs: large polygonal cells with granular, eosinophilic, and mitochondria-rich cytoplasm, prominent nucleoli, and markers of hepatocytes and cholangiocytes. In comparing expression levels of genes between the mouse tumor and non-tumor liver cells, we identified changes similar to those detected in human FL-HCC, which included genes that affect cell cycle and mitosis regulation. Genomic analysis of mouse neoplasms induced by the *Dnajb1–Prkaca* fusion revealed a lack of mutations in genes commonly associated with liver cancers, as observed in human FL-HCC. **CONCLUSIONS:** Using CRISPR/Cas9 technology, we found generation of the *Dnajb1–Prkaca* fusion gene in wild-type mice to be sufficient to initiate formation of tumors that have many features of human FL-HCC. Strategies to block DNAJB1–PRKACA might be developed as therapeutics for this form of liver cancer.

Keywords: Liver Cancer; Protein Kinase A; PKA; Genomic Engineering; Mouse Model.

Fibrolamellar hepatocellular carcinoma (FL-HCC) is a rare form of liver cancer that typically arises in children and young adults with no history of cirrhosis or other liver diseases.[1] The cancer carries high mortality, with 5-year survival below 45%.[2] Surgery is presently the only effective therapy if the cancer is diagnosed before the occurrence of metastases, and long-term survival is jeopardized by tumor recurrence.[2] FL-HCC has pathodiagnostic features distinct from the predominant liver cancers, classical hepatocellular carcinoma (HCC), and cholangiocarcinoma, which include large eosinophilic and mitochondria-rich polygonal cells with prominent nucleoli and lamellar bands of fibrosis.[3,4] FL-HCC expresses markers for hepatic progenitor, biliary, and hepatocytic lineages; however, none of these are specific for this tumor.[5,6]

The molecular basis of FL-HCC has been enigmatic because none of the major drivers of other liver cancers, as for

[§]Authors share co-senior authorship.

Abbreviations used in this paper: CEA, carcinoembryonic antigen; CRISPR/Cas9, clustered regularly interspaced short palindromic repeats/CRISPR-associated 9; FACS, fluorescence-activated cell sorting; FL-HCC, fibrolamellar hepatocellular carcinoma; GFP, green fluorescent protein; gRNA, guide RNA; GSEA, gene set enrichment analysis; HepPar1, hepatocyte paraffin 1; HRP, horseradish peroxidase; IDAA, indel detection by amplicon analysis; PCR, polymerase chain reaction; PKA, cAMP-dependent protein kinase A; SNVs, single nucleotide variants; WES, whole-exome sequencing.

Most current article

0016-5085
https://doi.org/10.1053/j.gastro.2017.09.008

EDITOR'S NOTES

BACKGROUND AND CONTEXT

A somatic chromosomal deletion that generates a chimeric *DNAJB1–PRKACA* gene fusion has been repeatedly identified in patients with fibrolamellar hepatocellular carcinoma, but its role in liver tumorigenesis has never been demonstrated.

NEW FINDINGS

The *Dnajb1–Prkaca* gene fusion generated somatically in the liver of adult wild-type mice by CRISPR/Cas9 technique is sufficient to initiate tumorigenesis and to induce liver tumors with cytological, histological and molecular features of fibrolamellar hepatocellular carcinoma.

LIMITATIONS

This study did not identify a mechanism where by the gene fusion initiates tumorigenesis.

IMPACT

The study suggests DNAJB1–PRKACA as an attractive therapeutic target for developing therapies for fibrolamellar hepatocellular carcinoma.

instance *CTNNB1*, *TP53* or *KRAS*, have been found mutated in FL-HCC. Recently, however, a ~400 kilobase (Kb) somatic deletion on chromosome 19 was identified in primary tumor samples from FL-HCC patients.[7,8] The deletion involves breakpoints that are positioned within intron 1, or less frequently within exon 2, of *DNAJB1,* which encodes a heat shock 40 protein family member, and within intron 1 of *PRKACA*, which encodes the adenosine 3′,5′-monophosphate (cAMP)-dependent protein kinase A (PKA) catalytic subunit alpha. The deletion generates a fusion gene encompassing exon 1 (and in fewer cases a portion of exon 2) of *DNAJB1* and exons 2–10 of *PRKACA*, producing a chimeric protein that retains PKA kinase activity.[7,8] Interestingly, the fusion gene is the only known recurrent genomic aberration in FL-HCC, where it has been identified in 80–100% of patients in various studies. By contrast, this aberration has not been reported in any other cancer.[7,9,10] Mutations in other genes have been detected in FL-HCC tumors along with the *DNAJB1–PRKACA* alteration.[8,11,12] However, at present, it remains to be established whether any of the genes found mutated in FL-HCC, most notably the *DNAJB1– PRKACA* fusion, may have a causative role.

Determining if *DNAJB1–PRKACA* is capable of initiating tumor formation is an outstanding question regarding the molecular basis of FL-HCC because this would establish the principal genetic origin of this cancer and identify the fusion protein as a candidate for new targeted therapies. To address this issue, we engineered the first FL-HCC mouse model by using the CRISPR/Cas9 technique (clustered regularly interspaced short palindromic repeats/CRISPR-associated 9) to elicit in mice the ~400 Kb chromosomal deletion that creates the *DNAJB1–PRKACA* fusion in patients. In addition to modeling the exact genomic alteration, we took several other measures to better mimic human FL-HCC. First, because *DNAJB1–PRKACA* mutation is somatic, we engineered this alteration in the liver of young adult mice through hydrodynamic tail vein delivery of the CRISPR/Cas9 reagents. Second, because we anticipated a low efficiency of the complex engineering task, we mirrored the stochastic and isolated mutational events that occur naturally during tumor formation. Third, because FL-HCC arises in healthy liver, we did not challenge the mice with any liver toxin, as for example CCl_4, which is otherwise frequently used to enhance liver cancer by damaging the liver and mimicking liver disease.[13] Finally, to best test *DNAJB1–PRKACA* as a potentially sole genetic driver, we engineered the aberration in a wild-type mouse genetic background, nor did we treat the mice with any mutagen such as Diethylnitrosamine (DEN), which is often used to increase tumor susceptibility and produce a cancer phenotype, when testing a new, candidate cancer gene in genetically engineered mouse models.[13]

Strikingly, the *Dnajb1–Prkaca* engineered mice developed tumors with high frequency that replicated human FL-HCC, as scored on several cytological and histological parameters. Furthermore, similar to human FL-HCC, we found no evidence of other plausible co-driver mutations in *Dnajb1–Prkaca*–elicited tumors.

Our findings demonstrate that the *DNAJB1–PRKACA* genomic alteration is sufficient to initiate and progress oncogenic transformation in FL-HCC. Together with the presence of the gene fusion in nearly all FL-HCC patients, our data strongly supports *DNAJB1–PRKACA* as the driver and specific diagnostic biomarker in FL-HCC. Furthermore, the fusion may constitute a promising and possibly sole candidate for targeted therapies in this cancer.

Materials and Methods

Generation of gRNA Constructs for Engineering the Dnajb1–Prkaca *Fusion*

Three guide (g)RNAs were designed to target intron 1 of either mouse *Dnajb1* or mouse *Prkaca* and introduced into pX330-U6-chimeric_BB-CBh-hSpCas9 vector that co-expresses gRNA driven by U6 promoter and Cas9 driven by chicken β-actin hybrid promoter[14] (Addgene plasmid #42230). Neuro-2a cells were transfected with the individual pX330 gRNA/Cas9 constructs along with empty pSpCas9(BB)-2A-GFP vector[15] at a 6:1 molecular ratio to mark transfected cells with GFP (green fluorescent protein), using X-tremeGENE HP transfection reagent according to the manufacturer's instructions (Sigma-Aldrich, St. Louis, MO). Two days post-transfection, we analyzed the efficiency of the gRNA designs using our protocol for genome editing using FACS (fluorescence-activated cell sorting) enrichment of nuclease expressing cells and indel detection by amplicon analysis (IDAA).[16] Briefly, the top 10% most GFP fluorescent cells were isolated by FACS and lysed to 2000 cells/μL in QuickExtract DNA extraction solution (Epicentre, Madison, WI). One-μL cell extract was used as template in a tri-primer genomic polymerase chain reaction (PCR) with locus-specific IDAA Fwd and Rev primers that amplified the gRNA target site and a common FamFwd primer identical to an overhang on the Fwd primer,

which rendered the amplicons fluorescent (sequences of primers used in this study are provided in Supplementary Table 1). Subsequent analysis of amplicons in a 3500 Genetic Analyzer (Thermo Fisher) revealed the size and frequency of insertion and deletion (indel) mutations elicited by the gRNA designs.

To test the ability of the gRNA constructs to generate the Dnajb1–Prkaca fusion, Neuro-2a cells were co-transfected with combinations of pX330 pairs targeting intron 1 of *Dnajb1* and *Prkaca*, using X-tremeGENE HP transfection reagent. Three days post-transfection, total RNA was extracted using QIAshredder spin columns (Qiagen, Ballerup, Denmark) and RNeasy Mini Kits (Qiagen). Total RNA was reverse transcribed using TaqMan Reverse Transcription Reagents (Thermo Fisher Scientific, Waltham, MA) and analyzed by PCR using the primers Dnajb1–RT-Fwd and Prkaca-RT-Rev that amplify the junction of the *Dnajb1–Prkaca* fusion cDNA. In addition, genomic DNA was extracted and PCR amplified with the primers Dnajb1–Fwd1 and Prkaca–Rev1 that amplify the *Dnajb1–Prkaca* junction and resulting PCR products were cloned and Sanger sequenced to determine the sequence of the CRISPR/Cas9-induced genomic breakpoint. Amplicons were further analyzed by IDAA using the primers Dnajb1–intron1-IDAA-Fwd and Prkaca–intron1-IDAA-Rev to determine the number and frequency of different fusion alleles present in the population.

CRISPR/Cas9 Engineering of Dnajb1–Prkaca *in the Adult Mice Liver*

The pair of pX330 gRNAs that appeared most optimal with respect to generating the *Dnajb1–Prkaca* fusion in vitro was delivered to the liver of adult mice via hydrodynamic tail vein injection, which was performed essentially as previously described.[17,18] Briefly, 8-week-old female FVB/N mice (FVB/NRj, Janvier Labs, Le Genest Saint Isle, France) were anesthetized with isoflurane (Abbott, Copenhagen, Denmark) and hydrodynamically injected within 5–8 seconds with 50 μg of each pX330 gRNA plasmid suspended in a volume of Ringer's solution corresponding to approximately 8% (vol/wt) of their body weight. The control cohort was injected with 100 μg of empty pX330 vector expressing Cas9 only. Animal housing and approvals are described in the Supplementary Materials and Methods.

Histology

Livers were fixed in 10% neutral buffered formalin (Lillies fixative) for 24 hours at 4°C, submersed in 70% ethanol for 24–48 hours, dehydrated in ethanol and xylene in a tissue processor, and then embedded in paraffin. The livers were cut into 3–5-μm thick sections that were mounted onto glass slides and deparaffinized and rehydrated by standard procedures. Sections were then either stained with H&E, with PicroSirius red, with periodic-acid Schiff reagent with or without pretreatment with diastase or subjected to immunohistochemistry using the following antibodies and conditions: rabbit monoclonal anti-cytokeratin 19 (1:200, ab52625; Abcam, Cambridge, United Kingdom) and rabbit anti-Ki67 (1:100, ab16667; Abcam) used with antigen retrieval in citrate buffer, pH 6.0 for 20 minutes at 98°C. Rabbit monoclonal anti-cytokeratin 7 (1:100, ab181598; Abcam), rabbit polyclonal anti-carcinoembryonic antigen (1:30, ab33562; Abcam), rabbit polyclonal anti-carbamoyl phosphate synthetase-1 (HepPar-1) (1:50, ab3682; Abcam), rabbit polyclonal anti-glutamine synthetase (1:1000, ab73593; Abcam) used with antigen retrieval in Tris EGTA buffer, pH 9.0, for 15–20 minutes at 98°. A Shandon Sequenza slide rack system (Thermo Fisher Scientific) was used to incubate sections with primary antibodies overnight at 4°C and for 45 minutes at room temperature with EnVision+ System Labeled Polymer–horseradish peroxidase (HRP) anti-rabbit (#K4003, Dako, Glostrup, Denmark), according to manufacturer's instructions. Chromogen staining was performed using NovaRED HRP substrate kit (VWR International, Søborg, Denmark). All antibodies were diluted in Antibody Diluent with Background Reducing Components (Dako). Counterstaining was performed using Harris haematoxylin (Histolab, Askim, Sweden).

Genomic PCR of the Dnajb1–Prkaca *Fusion on Laser Capture Microdissected Tumors*

Parrafin-embedded livers were sectioned at 5 μm thickness, mounted on 1.0 PEN MembraneSlides (Zeiss, Jena, Germany) and stained with H&E. Desired tissue areas were microdissected onto CapSure HS LCM Caps (Thermo Fisher Scientific) in an Arcturus PixCell II laser capture microdissection system. Genomic DNA was extracted from the captured tissue through incubation of the tissue for 6 hours at 65°C in 10 μL proteinase K-containing extraction buffer followed by 10 minutes at 95°C using the Arcturus PicoPure DNA Extraction Kit (Thermo Fisher Scientific). One μL of the extract was used as template in a multiplex PCR that simultaneously amplified the genomic *Dnajb1–Prkaca* breakpoint to test for the presence of the fusion as well as a nearby region in *Prkaca* that was not affected by the editing, thereby serving as an internal PCR control. PCR conditions are provided in the Supplementary Materials and Methods.

Additional methods can be found in the Supplementary Materials and Methods.

Results

CRISPR/Cas9-mediated engineering of Dnajb1–Prkaca *In Vitro and In Vivo*

In the mouse genome, *Dnajb1* and *Prkaca* are located on chromosome 8 in a region syntenic to human chromosome 19. To engineer in mice the complex chromosomal rearrangement that generates *DNAJB1–PRKACA* in human FL-HCC, we made use of CRISPR/Cas9 technology. In our approach, gRNAs were designed to target Cas9 to intron 1 of murine *Dnajb1* and intron 1 of murine *Prkaca* and thereby introduce DNA double-strand cuts in the regions, where chromosomal breaks occur in the vast majority of human FL-HCC analyzed (Figure 1*A*).[7] When co-introduced in cells, we expected the CRISPR/Cas9 reagents to excise the desired ~400 Kb genomic DNA fragment, and the cellular repair machinery to join the DNA ends and create the *Dnajb1–Prkaca* fusion, as occurring in human FL-HCC.

Thus, we first engineered constructs expressing Cas9 and guide (g)RNA in the pX330 vector[14] targeting either *Dnajb1* intron 1 or *Prkaca* intron 1 and assayed their efficiency in generating cuts at the respective target sites 2 days after their individual transfection into mouse Neuro-2a cells.

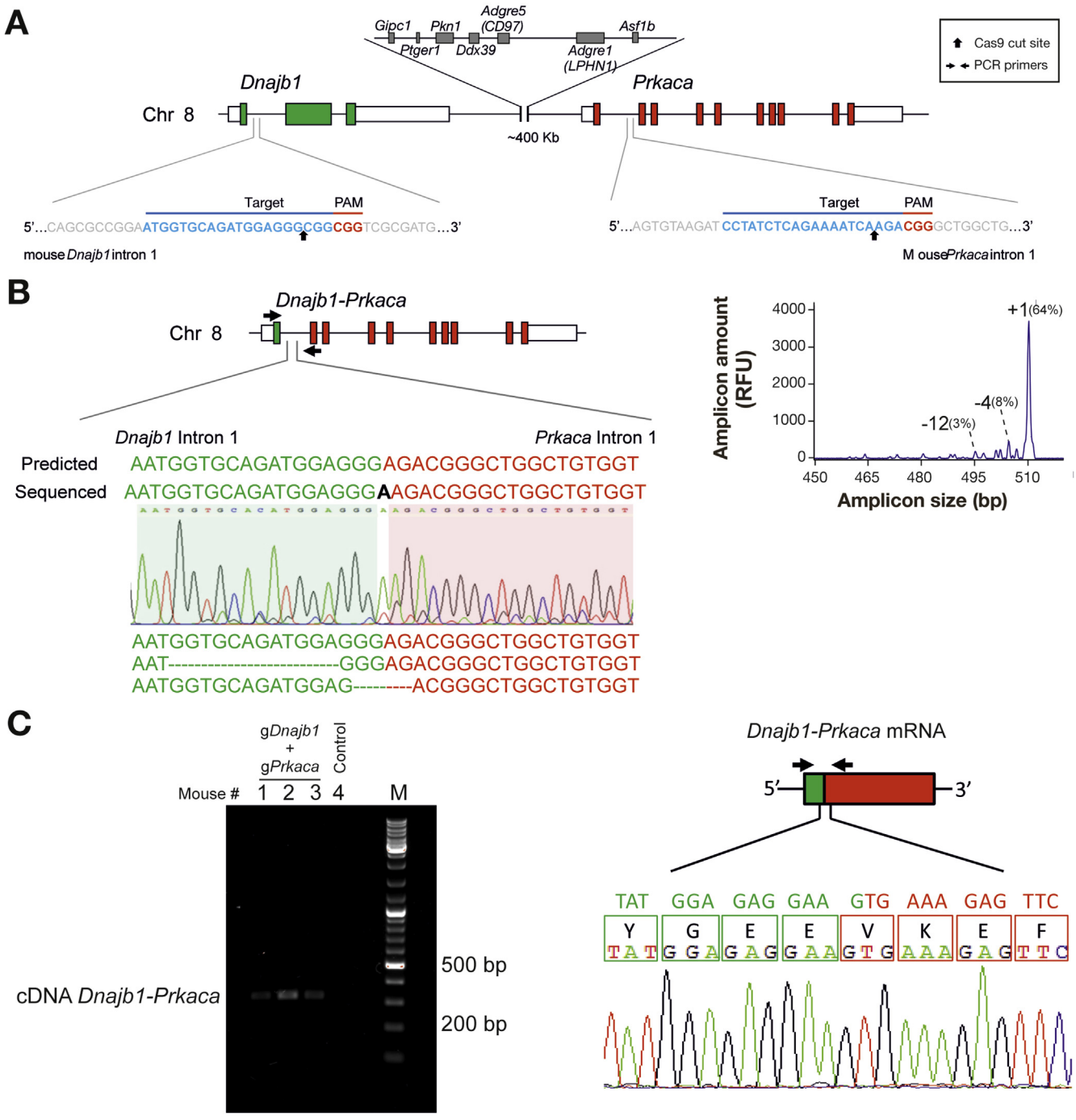

Figure 1. Generation of CRISPR/Cas9 reagents that engineer the *Dnajb1–Prkaca* fusion in vitro and in adult mouse liver. (*A*) In the mouse genome, *Dnajb1* and *Prkaca* are located on chromosome 8 in a region syntenic to human chromosome 19. The target sequences and locations of the gRNA pair used to engineer the *Dnajb1–Prkaca* fusion are shown. (*B*) Ability of the gRNA pair shown in (*A*) to engineer the *Dnajb1–Prkaca* fusion in transfected Neuro-2a cells. (*Left*) Schematic of the *Dnajb1–Prkaca* genomic fusion and location of primers (*arrows*) used to amplify the breakpoint. Sanger sequencing chromatogram and sequences for various fusion breakpoints are shown. "Predicted" sequence indicates gene fusion without any indel mutagenesis. (*Right*) IDAA profile showing the frequency of the various breakpoint amplicons. (*C*) Ability of the gRNA pair shown in (*A*) to engineer the *Dnajb1–Prkaca* fusion in the liver of hydrodynamically tail vein injected mice. (*Left*) *Dnajb1–Prkaca* specific PCR from cDNA derived from the liver of mice injected with the gRNA pair. (*Right*) Schematic of the fusion transcript and location of primers (*arrows*) used to amplify the fusion breakpoint. The Sanger sequencing chromatogram demonstrates an in-frame fusion transcript.

To this end, we used our recent protocol[16] to quantify the frequency of indel mutations generated by the cellular DNA repair machinery as a measure of the cutting efficiency of our CRISPR/Cas9 constructs (Supplementary Figure 1*A*). Next, we co-transfected the various construct pairs into Neuro-2a cells and assessed their ability to generate the *Dnajb1–Prkaca* fusion 3 days post-transfection. Analysis of genomic DNA and reverse-transcribed RNA by PCR and Sanger sequencing of the amplicons demonstrated the presence of the intended chromosomal rearrangement and the expression of the proper fusion transcript (Figure 1*B*, Supplementary Figure 1*B*).

Having confirmed the feasibility of our approach to engineer the desired chromosomal rearrangement in vitro, we combined our CRISPR/Cas9 reagents with hydrodynamic delivery in an attempt to create the *Dnajb1–Prkaca* aberration in the liver of young adult mice. Thus, we hydrodynamically tail vein injected 8-week-old mice with our most optimal CRISPR/Cas9 plasmid pair targeting *Dnajb1* and *Prkaca*, or with empty pX330 control plasmid. Three days post-injection, the mice were sacrificed and their livers analyzed. Genomic DNA and mRNA analyses showed the presence of the *Dnajb1–Prkaca* fusion and detectable levels of fusion transcript in mice injected with the CRISPR/Cas9 plasmid pair (Figure 1*C* and Supplementary Figure 1*C*). We estimated that the frequency of the *Dnajb1–Prkaca* genomic fusion was approximately 0.7–1.5 copy/100 cells in the CRISPR/Cas9 edited livers (data not shown).

The Dnajb1–Prkaca *Fusion Induces FL-HCC in Mice*

A cohort of 8-week-old wild-type mice was hydrodynamically tail vein injected with the CRISPR/Cas9 plasmid pair for generation of the *Dnajb1–Prkaca* aberration or with empty pX330 control plasmid. Mice were sacrificed 14 months post-injection at the time when some of the mice showed signs of distress and their livers analyzed for the presence of alterations. Twelve out of 15 (80%) CRISPR/Cas9-injected mice and 0 of 11 control-injected mice presented oncogenic lesions in the liver parenchyma that varied in size (Figure 2, Supplementary Figure 3). Mouse FL-HCC driven by the fusion showed most of the specific cytologic and histologic features of human FL-HCC, as illustrated by a large brownish and fully surfaced tumor (10–12 mm) shown in Figure 2*A*. As in human, mouse FL-HCC appears as a relatively well-circumscribed mass with pushing margin against the non-tumorous tissue, and composed of solid sheets and tightly packed cords and trabeculae of large polygonal hepatocyte-like cells separated by variably dilated sinusoids. Furthermore, tumor cells contained large nuclei with coarse chromatin and 1 or more prominent nucleoli (Figure 2*B* and 2*C*)[19,20], and their abundant cytoplasm was characteristically granular and eosinophilic in analogy with the "oncocyte-like" aspects of the mitochondria-rich cytoplasm in cells of human FL-HCC.[21] Indeed, ultrastructural analysis obtained by transmission electron microscopy confirmed the presence of tightly packed mitochondria in cells from mouse FL-HCC and also evidenced the characteristic nuclear morphology of these oncocytic hepatocytes[22,23] (Figure 2*D* and Supplementary Figure 2*A*). Additionally, tumor cells contained inclusions resembling the intracellular "pale bodies" as well as the hyaline globules often observed in human FL-HCC (Figure 2*C*, Supplementary Figure 2*B*), and accordingly, these globules contained material that was positive for the periodic acid-Schiff stain and sensitive to diastase enzymatic digestion (Figure 2*E*, and data not shown).[1] Importantly, the tumor was positive for the intended CRISPR/Cas9-induced *Dnajb1–Prkaca* fusion and expressed the chimeric in-frame transcript, as demonstrated by genomic DNA and reverse transcribed mRNA sequencing (Supplementary Figure 2*C*). No sign of off-target cutting elicited by the CRISPR/Cas9 tools was evident in the top-ranking predicted off-target sites for both gRNAs,[24] as assessed by IDAA (Supplementary Figure 2*D* and data not shown).

The smaller neoplastic lesions (<1 mm) were also characterized by the distinctive "oncocytic" hepatocytes described in human FL-HCC. As observed for the large cells that constitute both human and murine FL-HCC, the "oncocytic" hepatocyte-like cells in these lesions were also large, also contained granular eosinophilic-orange cytoplasm, large nuclei, and prominent nucleoli (Figure 2*F* and Supplementary Figure 3*B*). Such oncocytic cells were also present in transition areas between the large tumor shown in Figure 2*A* and the surrounding non-tumorous tissue, hence supporting the notion that these foci represent precursor lesions for FL-HCC. The small lesions often showed various degrees of leukocyte infiltration inside and around the foci (Figure 2*F* and Supplementary Figure 3*B*). All the large and small *Dnajb1–Prkaca*-elicited lesions showed the cytologic characteristics of FL-HCC described above. Only 1 lesion, in fact, contained premalignant clear cells intermingled with oncocytic hepatocytes with prominent nucleoli and eosinophilic cytoplasm (Supplementary Figure 3*C*), in accordance with the observation that FL-HCC may occasionally appear as a mixed-FL-HCC, which has also been reported positive for the fusion.[25] Genomic DNA analysis of laser capture microdissected small lesions confirmed the presence of the oncogenic *Dnajb1–Prkaca* aberration (Supplementary Figure 3*D*).

PicroSirius red staining for collagen showed mild thickening of the collagen connective tissue network accompanying the tumor cells (Figure 3*A*), whereas the non-tumorous liver parenchyma was completely devoid of fibrotic change (Supplementary Figure 4*A*). The collagen bands in murine FL-HCC were not as thick as in human FL-HCC and no large, central collagen scar was observed, which however is consistent with the limited tendency of mouse liver to develop collagen fibrosis without chemical challenge.[26]

Immunohistochemical characterization showed that mouse FL-HCC elicited by *Dnajb1–Prkaca* expresses both hepatocyte and cholangiocyte markers, as reported for

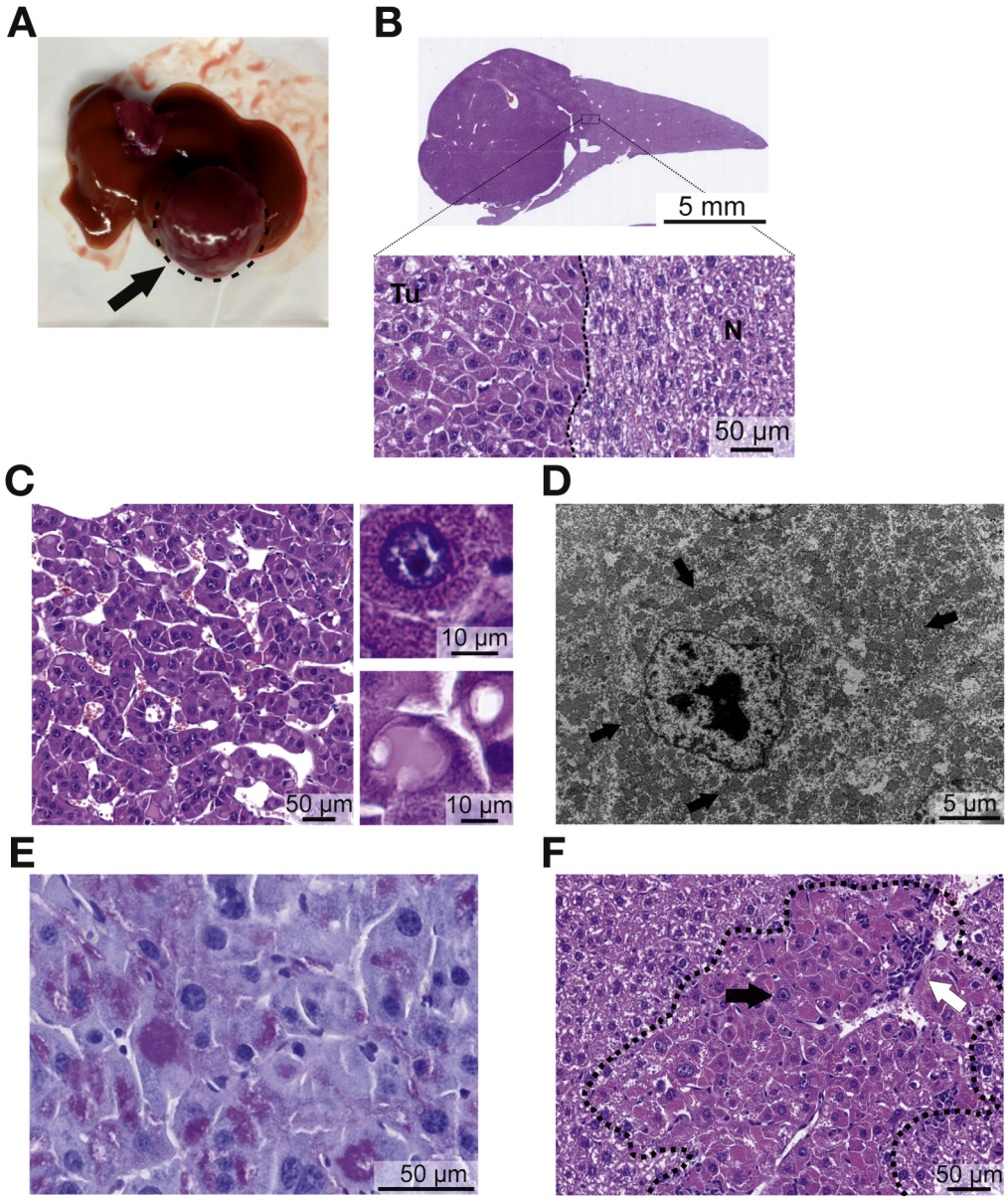

Figure 2. The *Dnajb1–Prkaca* fusion induces FL-HCC in mice. Representative macroscopic and microscopic images of mouse FL-HCC elicited by *Dnajb1–Prkaca.* (*A*) Macroscopic image of a tumor (*arrow*). (*B*) Whole-scan H&E image and magnification showing tumor (Tu)-non-tumor (N) border. (*C*) Microscopic H&E image of tumor area showing trabeculae of tumor cells separated by variably dilated sinusoids. (*Upper inset*) Detail of an "oncocytic" tumor cell with granular eosinophilic cytoplasm and large nucleus with prominent nucleolus. (*Lower inset*) Detail of "pale body" and hyaline globulus. (*D*) Transmission electron micrograph of tumor cell showing cytoplasm packed with mitochondria (*arrows*) and nucleus with prominent nucleolus and coarse chromatin. (*E*) Periodic acid-Schiff staining of hyaline globules. (*F*) Small neoplastic lesion with large oncocytic cells with granular eosinophilic cytoplasm and prominent nucleoli (*black arrow*) and leukocyte infiltration (*white arrow*).

human FL-HCC.[5,11] Indeed, mouse FL-HCC was positive for the hepatocytic markers hepatocyte paraffin 1 (HepPar1) and carcinoembryonic antigen (CEA) with a canalicular distribution (Figure 3*B* and *C*), as frequently observed in human FL-HCC.[5,11] Furthermore, mouse FL-HCC showed scattered expression of cytokeratin 7 and cytokeratin 19 (Figure 3*D* and *E*), 2 markers that are frequently and occasionally expressed, respectively, by human FL-HCC,[5,11] whereas in normal liver these proteins are present only in the cholangiocytes of the bile ducts and in hepatic progenitor cells (Supplementary Figure 4*B* and *C*). Finally, mouse FL-HCC expressed glutamine synthetase (Figure 3*F*), which occurs in both HCC and cholangiocarcinoma with similar frequency,[27] whereas in normal liver only hepatocytes adjacent to the central vein are positive (Supplementary Figure 4*D*).

Molecular Analysis Supports Dnajb1–Prkaca *as the Key Driver of Initiation and Progression of FL-HCC*

To gain further insight into the mechanisms underlying neoplastic transformation induced by *Dnajb1–Prkaca*, we performed transcriptomic and genomic analyses of the lesions. RNA-seq analysis of total RNA isolated from a tumor where freshly frozen tissue was available and from freshly frozen tissue from control injected mouse livers confirmed the expression of the proper *Dnajb1–Prkaca* fusion transcript in the tumor, with juxtaposition of exon 1 of *Dnajb1* to exon 2 of *Prkaca* (Figure 4*A* and Supplementary Table 2). Gene set enrichment analysis (GSEA) of the differentially expressed genes between tumor and liver control against the Molecular Signatures Database (Broad Institute, C5.bp), revealed a robust

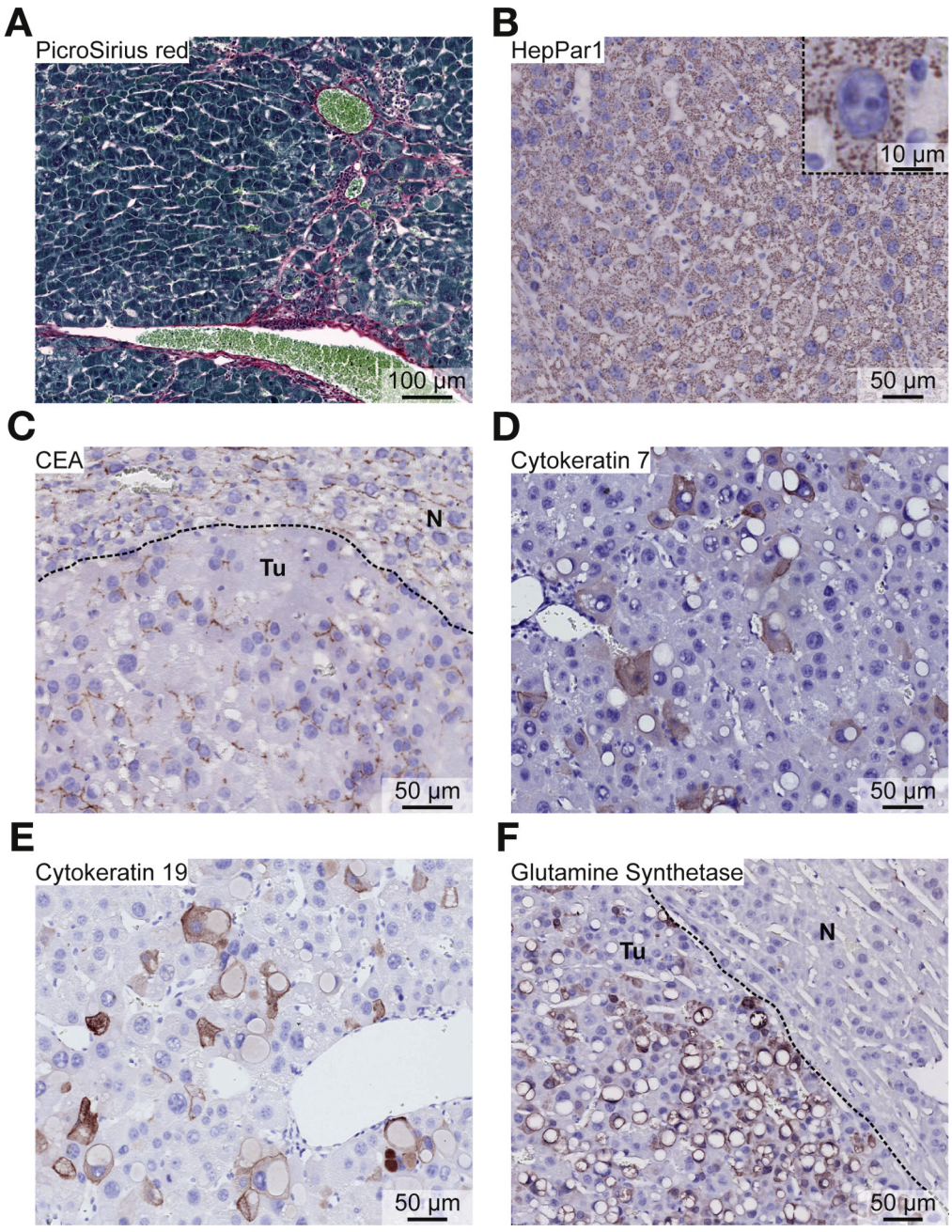

Figure 3. Histologic characterization of *Dnajb1–Prkaca* elicited mouse FL-HCC. (*A*) PicroSirius red staining showing mild collagen fibrosis between tumor cells. (*B*) Tumor cells express HepPar1. (*Inset*) Detail of a tumor cell expressing HepPar1 with mitochondrial localization and illustrating the mitochondria-rich cytoplasm. (*C*) CEA staining showing canalicular distribution in tumor area (Tu), as well as in normal liver area (N). (*D*) Cytokeratin 7 expression in tumor area. (*E*) Cytokeratin 19 expression in tumor area. (*F*) Broad expression of glutamine synthetase by tumor cells (Tu), but not by hepatocytes of the normal liver area (N).

enrichment of genes in processes associated with cell cycle control and mitosis regulation, and a down-regulation of genes involved in regulation of metabolic processes (GSEA: false discovery rate (*P* value, <.05) (Supplementary Tables 3, 4, and 5). Further results for positively and negatively regulated enriched gene sets are presented in Supplementary Tables 6 and 7.

Several studies have contributed to the characterization of the transcriptomic profile of human FL-HCC by comparing expression data from tumor specimen with that of normal liver or with that of other liver cancers.[10,11,28–30] We compared the differentially expressed genes between mouse FL-HCC and normal mouse liver with those from 3 different human FL-HCC studies[8,11,29] and identified a strong enrichment (GSEA: familywise error rate adjusted *P* value, <.001) of mouse FL-HCC genes in the down-regulated and up-regulated gene sets from these human studies, thus further confirming the resemblance of mouse tumor to human FL-HCC (Supplementary Figure 5*A*). In particular, common differentially expressed genes between RNA-seq data from human[29] and mouse FL-HCC include directionally concordant genes involved in cell cycle and mitosis regulation processes (Figure 4*B*) (list of genes provided in Supplementary Tables 8 and 9). The mouse FL-HCC transcriptome also displayed a profile closest resembling that of mature hepatocytes as evidenced by a comparison

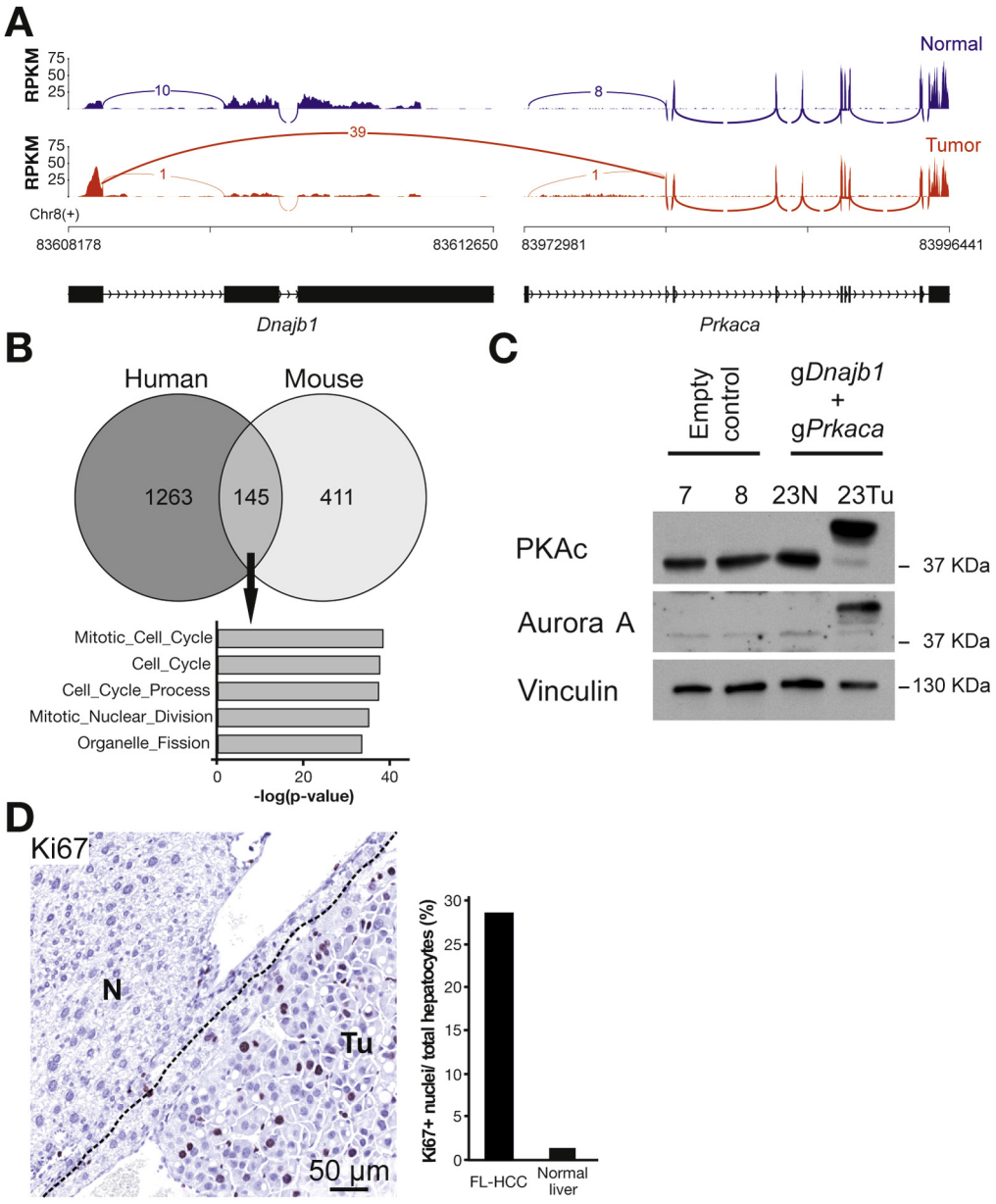

Figure 4. Molecular analysis of *Dnajb1–Prkaca* elicited mouse FL-HCC. (*A*) Sashimi plot of RNA-seq read coverage for *Dnajb1* and *Prkaca* in normal liver and mouse FL-HCC. Peaks depict reads per kilobase per million reads mapped (RPKM). Arcs depict reads spanning splice junctions. (*B*) Venn Diagram showing overlap of differentially expressed genes between human (Simon et al[29]) and mouse FL-HCC. Differentially expressed genes for mouse FL-HCC were defined by a BaseMean value >25 and log2FC >1.5 over normal liver. Gene Ontology Biological Process (MSigDB, c5.bp) is shown for the 145 common differentially expressed genes, showing enrichment of mitosis and proliferation genes. (*C*) Immunoblotting of tissue lysates from mouse FL-HCC tumor (Tu), adjacent normal liver (N) or livers from control mice. PKAc, immunoblotting using an antibody raised against the catalytic subunit alpha of PKA. Vinculin is used as loading control. (*D*) Ki67-staining of tumor cells (Tu) and adjacent normal tissue (N). Bars represent quantification of Ki67-positive cells/number of hepatocytes.

between our dataset to mouse RNA-seq data available in the literature[31] (Supplementary Figure 5*B*).

Notably, human FL-HCC was reported to express high levels of the cytokinesis and mitosis regulator Aurora kinase A[29,30] and a clinical trial is ongoing to test the efficacy of its inhibition in FL-HCC patients.[32] Our RNA-seq data and immunoblotting of tissue lysate from mouse FL-HCC tumor showed high expression of Aurora kinase A, as compared with the non-tumorous area of the liver and control-injected livers (Supplementary Table 3 and Figure 4*C*) and, as expected, expression of the DNAJB1–PRKACA fusion protein, thus further corroborating the rationale of targeting Aurora kinase A in clinical trials. Moreover, tumors showed a high proliferation index revealed by Ki67 staining, as opposed to normal hepatocytes in the adjacent non-tumorous areas (Figure 4*D*, Supplementary Figure 3*A*).

Human FL-HCC has been concordantly shown to have a relative stable genome with fewer mutations than other liver cancers and, with the exception of the *DNAJB1–PRKACA* fusion, no known liver cancer genes are recurrently altered.[8,11,12,33] These findings prompted us to analyze the mutational load of our CRISPR/Cas9 generated mouse FL-HCC. We therefore performed Whole-exome sequencing (WES) of paired normal liver and mouse FL-HCC (for 1 larger and 1 smaller tumor) to identify genomic alterations that could have contributed to tumorigenesis instigated by *Dnajb1–Prkaca*. A total of 80 single nucleotide variants (SNVs) and 1 deletion were identified in the larger tumor (Supplementary Figure 6*A* and Supplementary Table 10): of these, 35 were non-synonymous (Supplementary Figure 6*B*) that we scored for their potentially damaging effect using Polyphen2.[34] Importantly, only 1 gene with a damaging SNV

had a frequency of the mutant allele above 15% (ie, *Aldh2*, which is involved in alcohol catabolism). Although an *ALDH2* polymorphism (*rs 671*, missense mutation E457K) has been associated with increased susceptibility to alcohol-induced gastrointestinal cancer in East Asians,[35] it is perhaps not so likely that the *Aldh2* SNV identified here contributes to *Dnajb1–Prkaca*-elicited FL-HCC in the present mouse setting. We Sanger sequenced the mutated region of most of those genes expressed, as evidenced by the RNA-seq data, and harboring predicted deleterious mutations, and confirmed the presence of SNVs in 8 cases (Supplementary Table 10). We also confirmed by IDAA the 3 basepair intronic deletion identified in 1 gene (Supplementary Figure 6*C*). Importantly, none of the mutated genes were reported mutated in any of the human FL-HCC genomic studies, nor have these genes been found consistently mutated in human liver cancers or are obvious cancer drivers (Supplementary Table 10). The mutational load of the smaller tumor was characterized by fewer SNVs (9) than the larger tumor described above, and it confirmed the absence of recurrent mutations or mutations in known cancer genes in FL-HCC induced by *Dnajb1–Prkaca*, and supported the idea that the number of mutations in a tumor increases as a consequence of its evolution (Supplementary Table 11). Interestingly, only 1 indel mutation site with no resemblance to the gRNAs used was detected by the WES, demonstrating that CRISPR/Cas9 off-target mutagenesis had not occurred within the exome of the tumors. Lastly, of some of the most prevalently mutated genes in other liver cancers (*CTNNB1*, *TP53* and *KRAS*)[11] or in mouse models of liver cancers[13] (*Hras*), none were found to be mutated by targeted analysis of the smaller lesions that we analyzed.

Discussion

The aim of this study was to determine if the *DNAJB1–PRKACA* fusion is oncogenic and by inference, is the causative mutation of FL-HCC. With the emerging recognition that *DNAJB1–PRKACA* occurs in most, if not all FL-HCC patients, the functional demonstration of *DNAJB1–PRKACA* as driver would establish the genetic origin of this cancer.

We provided this evidence by the stringent approach of engineering in adult mouse liver the same genomic *Dnajb1–Prkaca* alteration that occurs in human FL-HCC. To this end, we exploited the powerful CRISPR/Cas9 technology, which was recently used to engineer the complex genomic rearrangement that creates the well-established oncogenic *EML4-ALK* fusion in mouse models of human lung cancer.[36,37] Moreover, a key point of our study is that we engineered *Dnajb1–Prkaca* in wild-type mice and without administration of any mutagens, to conclude, upon tumor formation, that *DNAJB1–PRKACA* is the main driving mutation. Finally, our engineering of the aberration in a healthy mouse liver and, at a low frequency, are important additional features of our study that mimic the stochastic and rare events leading to tumor initiation in FL-HCC patients in absence of other liver disease. The development of neoplastic lesions in the majority of our CRISPR/Cas9-engineered mice demonstrated that *Dnajb1–Prkaca* is sufficient to induce FL-HCC and thus is the main genetic event that initiates this cancer. The tumor latency of >1 year in our FL-HCC model is not unusual for a single genetic alteration in mouse liver cancer models,[13] and is consistent with the notion that FL-HCC is considered to be a slowly progressing liver cancer in humans.[21]

Importantly, the lesions induced by *Dnajb1–Prkaca* in mice had a high resemblance with human FL-HCC. Gross-anatomically, the tumors were well circumscribed from adjacent normal liver tissue as seen for human FL-HCC. Perhaps most strikingly, the cytologic characteristics of mouse FL-HCC were highly similar to those of human FL-HCC, which are used as major diagnostic features in the clinic (reviewed in Torbenson[1], and in Ward and Waxman[33]). Indeed, mouse lesions were composed of unusually large, polygonal tumor cells, often presenting prominent macronucleoli and with an abundant granular eosinophilic cytoplasm characteristic of oncocytic hepatocytes. The cytologic appearance of these oncocytic hepatocytes is because of the presence of densely packed mitochondria, as evidenced by ultrastructural examination of both human and mouse FL-HCC in electron microscopy studies. Mouse lesions also showed, as observed in nearly half of human FL-HCC, hyaline globules and round cytoplasmatic inclusions known as "pale bodies."[1] It therefore appears that *Dnajb1–Prkaca* has the cell-autonomous capacity to elicit all the characteristics of the FL-HCC cell phenotype, both in mouse and human.

In one respect mouse FL-HCC did not fully recapitulate the human tumor. Although collagen fibrosis was observed, it was considerably less pronounced than in human FL-HCC, where it sometimes forms a large, central scar. The limited fibrosis may not be surprising because mouse livers are known to display an attenuated fibrotic response, as observed in mouse models of cancer as well as liver fibrosis.[13] Little is known about how fibrosis is elicited in FL-HCC, nor is there any evidence that the collagen deposition has any role in the progression of FL-HCC. The present study suggests that FL-HCC arises and progress through a cell autonomous action of *Dnajb1–Prkaca* within the tumor cells, which does not depend on fibrosis in the tumor.

Mouse FL-HCC also resembles human FL-HCC by expressing both hepatocytic and cholangiocytic markers as evidenced by immunohistochemical characterization. Although widely used in clinical practice, none of the proposed markers are actually specific for FL-HCC and their diagnostic significance is therefore limited.[38] Mouse FL-HCC expressed high levels of hepatocytes markers (CEA and HepPar1) and displayed scattered positivity for the biliary epithelium marker cytokeratin 7 and a stronger staining for cytokeratin 19, a marker associated with both biliary differentiation and hepatic progenitors. Mouse FL-HCC failed to show staining for CD68, which has been shown to be expressed in human tumors (data not shown).[39]

Transcriptomic analysis of mouse FL-HCC revealed similarities with human FL-HCC as well as differences. In fact, we did not identify in our dataset previously reported

overexpressed genes associated with a neuroendocrine signature, as these genes were either expressed at a very low level or were not differentially expressed. An exception was carboxypeptidase, which we found up-regulated (Supplementary Table 3), in agreement with Xu et al.[8] However, although overexpression of some of these genes has been observed in several studies,[8,11,28,29] gene signatures have failed to consistently mark FL-HCC as a tumor of neuroendocrine origin.[29,33] Species differences in gene expression between human and mouse may explain the lack of select FL-HCC features, most notably the lamellar bands of fibrosis, in the murine tumor. However, a strong enrichment in directionally concordant differentially expressed genes in mouse and human tumor was evidenced by cross-species GSEA.

In mouse FL-HCC we confirmed the increased expression of Aurora kinase A, a mitotic serine/threonine kinase involved in cell cycle progression and implicated in tumorigenesis, which was recently reported up-regulated in 2 human FL-HCC studies.[29,30] This finding may be important in light of the ongoing clinical trial aimed at testing Aurora kinase A inhibition in FL-HCC patients; also in that it identifies a common pathologic event initiated by *DNAJB1–PRKACA* in both human and mouse FL-HCC, which represents an attractive therapeutic target.[40]

It remains unclear to what extent, if any, mutations other than the *DNAJB1–PRKACA* aberration contribute to FL-HCC. Prior to the discovery of *DNAJB1–PRKACA*, driver genes were searched for using comparative genomic amplification analyses or focused analyses of genes known to underlie other liver cancers, which, however, did not identify any plausible FL-HCC drivers.[33] After the discovery of *DNAJB1–PRKACA*, 2 studies performed whole-exome sequencing on a single tumor containing the fusion,[8,11] the latter extending the analysis of a few mutated genes to a larger FL-HCC tumor collection. The 2 studies identified relatively few coding mutations (11 and 90), which showed no overlap, were infrequently considered damaging, and did not affect known cancer genes, except for *BRCA2,* which was found mutated in 4.2% of FL-HCC samples in the extended analysis. Another study performed whole-genome sequencing of 10 FL-HCC patients and found no recurrent structural variants other than *DNAJB1–PRKACA*, few coding mutations per tumor (a median of 6) and some genes being recurrently mutated of which the significance was unclear.[12] The authors concluded that the lack of second-hit mutation in FL-HCC makes the DNAJB1–PRKACA fusion protein the best target for diagnostic and therapeutic advancement. Our study agrees with the human studies, as we found no relevant coding mutations in known driver genes for liver cancers or other malignancies.

Regardless of the possible involvement of other genes, our finding that *DNAJB1–PRKACA* is sufficient to elicit FL-HCC combined with its ubiquitous presence in FL-HCC patients firmly establish *DNAJB1–PRKACA* as the dominant genetic driver of this cancer. Indeed, testing of DNAJB1–PRKACA mRNA or protein as a drug target in FL-HCC is highly warranted.[38] DNAJB1–PRKACA could prove as excellent a drug target as the BCR-ABL1 fusion in chronic myeloid leukemia, where a single, oncogenic event elicits and drives the disease and predicts a very favorable response to its inhibition.[41] This scenario would require that, once formed, FL-HCC tumors remain addicted to DNAJB1–PRKACA for growth and survival. FL-HCC mouse models generated as described here, along with a recently established FL-HCC transplantable tumor line,[42] might constitute preclinical settings where the DNAJB1–PRKACA fusion could be tested as a drug target in FL-HCC.

In summary, we report the first CRISPR/Cas9-engineered mouse model of liver cancer generated somatically by a single oncogenic modification in otherwise wild-type mice and without administration of toxin or carcinogen. Furthermore, we describe the first mouse model of FL-HCC, notably one that replicates to a high extent the genotype and phenotype associated with this human cancer. Importantly, our study demonstrates that the recently identified *DNAJB1–PRKACA* fusion is the cause of FL-HCC, and is responsible for oncogenic transformation and major pathodiagnostic features of this cancer. Our findings thereby provide strong support for DNAJB1–PRKACA as a target for new therapies in FL-HCC and our mouse model may be useful to study the initiation and progression of FL-HCC as well as pre-clinical testing of new treatments.

Supplementary Material

Note: To access the supplementary material accompanying this article, visit the online version of *Gastroenterology* at www.gastrojournal.org, and at https://doi.org/10.1053/j.gastro.2017.09.008.

References

1. Torbenson M. Fibrolamellar carcinoma: 2012 update. Scientifica (Cairo) 2012;2012:743790.
2. Kakar S, Burgart LJ, Batts KP, et al. Clinicopathologic features and survival in fibrolamellar carcinoma: comparison with conventional hepatocellular carcinoma with and without cirrhosis. Mod Pathol 2005;18:1417–1423.
3. Craig JR, Peters RL, Edmondson HA, et al. Fibrolamellar carcinoma of the liver: a tumor of adolescents and young adults with distinctive clinico-pathologic features. Cancer 1980;46:372–379.
4. El-Serag HB, Davila JA. Is fibrolamellar carcinoma different from hepatocellular carcinoma? A US population-based study. Hepatology 2004;39:798–803.
5. Ward SC, Huang J, Tickoo SK, et al. Fibrolamellar carcinoma of the liver exhibits immunohistochemical evidence of both hepatocyte and bile duct differentiation. Mod Pathol 2010;23:1180–1190.
6. Abdul-Al HM, Wang G, Makhlouf HR, et al. Fibrolamellar hepatocellular carcinoma: an immunohistochemical comparison with conventional hepatocellular carcinoma. Int J Surg Pathol 2010;18:313–318.
7. **Honeyman JN, Simon EP, Robine N**, et al. Detection of a recurrent DNAJB1–PRKACA chimeric transcript in fibrolamellar hepatocellular carcinoma. Science 2014;343:1010–1014.

8. Xu L, Hazard FK, Zmoos AF, et al. Genomic analysis of fibrolamellar hepatocellular carcinoma. Hum Mol Genet 2015;24:50–63.
9. Graham RP, Jin L, Knutson DL, et al. DNAJB1–PRKACA is specific for fibrolamellar carcinoma. Mod Pathol 2015; 28:822–829.
10. Dinh TA, Vitucci EC, Wauthier E, et al. Comprehensive analysis of The Cancer Genome Atlas reveals a unique gene and non-coding RNA signature of fibrolamellar carcinoma. Sci Rep 2017;7:44653.
11. Cornella H, Alsinet C, Sayols S, et al. Unique genomic profile of fibrolamellar hepatocellular carcinoma. Gastroenterology 2015;148:806–818.e10.
12. Darcy DG, Chiaroni-Clarke R, Murphy JM, et al. The genomic landscape of fibrolamellar hepatocellular carcinoma: whole genome sequencing of ten patients. Oncotarget 2015;6:755–770.
13. Heindryckx F, Colle I, Van Vlierberghe H. Experimental mouse models for hepatocellular carcinoma research. Int J Exp Pathol 2009;90:367–386.
14. **Cong L, Ran FA**, Cox D, et al. Multiplex genome engineering using CRISPR/Cas systems. Science 2013; 339:819–823.
15. **Ran FA, Hsu PD**, Wright J, et al. Genome engineering using the CRISPR-Cas9 system. Nat Protoc 2013; 8:2281–2308.
16. **Lonowski LA, Narimatsu Y, Riaz A, Delay CE**, et al. Genome editing using FACS enrichment of nuclease-expressing cells and indel detection by amplicon analysis. Nat Protoc 2017;12:581–603.
17. Zhang G, Budker V, Wolff JA. High levels of foreign gene expression in hepatocytes after tail vein injections of naked plasmid DNA. Hum Gene Ther 1999;10:1735–1737.
18. Dagnaes-Hansen F, Holst HU, Søndergaard M, et al. Physiological effects of human growth hormone produced after hydrodynamic gene transfer of a plasmid vector containing the human ubiquitin promotor. J Mol Med (Berl) 2002;80:665–670.
19. Torbenson M. Review of the clinicopathologic features of fibrolamellar carcinoma. Adv Anat Pathol 2007; 14:217–223.
20. Berman MA, Burnham JA, Sheahan DG. Fibrolamellar carcinoma of the liver: an immunohistochemical study of nineteen cases and a review of the literature. Hum Pathol 1988;19:784–794.
21. Hodgson HJ. Fibrolamellar cancer of the liver. J Hepatol 1987;5:241–247.
22. Payne CM, Nagle RB, Paplanus SH, et al. Fibrolamellar carcinoma of liver: a primary malignant oncocytic carcinoid? Ultrastruct Pathol 1986;10:539–552.
23. Farhi DC, Shikes RH, Silverberg SG. Ultrastructure of fibrolamellar oncocytic hepatoma. Cancer 1982; 50:702–709.
24. Haeussler M, Schönig K, Eckert H, et al. Evaluation of off-target and on-target scoring algorithms and integration into the guide RNA selection tool CRISPOR. Genome Biol 2016;17:148.
25. **Griffith OL, Griffith M, Krysiak K**, et al. A genomic case study of mixed fibrolamellar hepatocellular carcinoma. Ann Oncol 2016;27:1148–1154.
26. **Fujii T, Fuchs BC**, Yamada S, et al. Mouse model of carbon tetrachloride induced liver fibrosis: histopathological changes and expression of CD133 and epidermal growth factor. BMC Gastroenterol 2010; 10:79.
27. Lagana SM, Moreira RK, Remotti HE, et al. Glutamine synthetase, heat shock protein-70, and glypican-3 in intrahepatic cholangiocarcinoma and tumors metastatic to liver. Appl Immunohistochem Mol Morphol 2013; 21:254–257.
28. **Malouf GG, Job S**, Paradis V, et al. Transcriptional profiling of pure fibrolamellar hepatocellular carcinoma reveals an endocrine signature. Hepatology 2014; 59:2228–2237.
29. Simon EP, Freije CA, Farber BA, et al. Transcriptomic characterization of fibrolamellar hepatocellular carcinoma. Proc Natl Acad Sci U S A 2015;112:E5916–E5925.
30. Sorenson EC, Khanin R, Bamboat ZM, et al. Genome and transcriptome profiling of fibrolamellar hepatocellular carcinoma demonstrates p53 and IGF2BP1 dysregulation. PLoS One 2017;12:e0176562.
31. Lee DH, Park JO, Kim TS, et al. LATS-YAP/TAZ controls lineage specification by regulating TGFβ signaling and Hnf4α expression during liver development. Nat Commun 2016;7:11961.
32. ClinicalTrials.gov. A multi-center, open-label study of oral enmd-2076 for the treatment of patients with advanced fibrolamellar carcinoma. Available at: https://clinicaltrials.gov/ct2/show/NCT02234986?term=fibrolamellar&rank=2.
33. Ward SC, Waxman S. Fibrolamellar carcinoma: a review with focus on genetics and comparison to other malignant primary liver tumors. Semin Liver Dis 2011; 31:61–70.
34. **Adzhubei IA, Schmidt S, Peshkin L**, et al. A method and server for predicting damaging missense mutations. Nat Methods 2010;7:248–249.
35. Cui R, Kamatani Y, Takahashi A, et al. Functional variants in ADH1B and ALDH2 coupled with alcohol and smoking synergistically enhance esophageal cancer risk. Gastroenterology 2009;137:1768–1775.
36. Maddalo D, Manchado E, Concepcion CP, et al. In vivo engineering of oncogenic chromosomal rearrangements with the CRISPR/Cas9 system. Nature 2014; 516:423–427.
37. **Blasco RB, Karaca E**, Ambrogio C, et al. Simple and rapid in vivo generation of chromosomal rearrangements using CRISPR/Cas9 technology. Cell Rep 2014; 9:1219–1227.
38. Riggle KM, Turnham R, Scott JD, et al. Fibrolamellar hepatocellular carcinoma: mechanistic distinction from adult hepatocellular carcinoma. Pediatr Blood Cancer 2016;63:1163–1167.
39. Ross HM, Daniel HD, Vivekanandan P, et al. Fibrolamellar carcinomas are positive for CD68. Mod Pathol 2011; 24:390–395.
40. Katsha A, Belkhiri A, Goff L, et al. Aurora kinase A in gastrointestinal cancers: time to target. Mol Cancer 2015;14:106.

41. Rosti G, Castagnetti F, Gugliotta G, et al. Tyrosine kinase inhibitors in chronic myeloid leukaemia: which, when, for whom? Nat Rev Clin Oncol 2017;14:141–154.
42. **Oikawa T, Wauthier E**, Dinh TA, et al. Model of fibrolamellar hepatocellular carcinomas reveals striking enrichment in cancer stem cells. Nat Commun 2015;6:8070.

Author names in bold designate shared co-first authorship.

Received April 12, 2017. Accepted September 9, 2017.

Reprint requests
Address requests for reprints to: Francesco Niola, PhD, Biotech Research and Innovation Centre, Faculty of Health and Medical Sciences, University of Copenhagen, Ole Maaloes Vej 5, Copenhagen DK-2200, Denmark. e-mail: francesco.niola@outlook.com; or Morten Frödin, PhD, Biotech Research and Innovation Centre, Faculty of Health and Medical Sciences, University of Copenhagen, Ole Maaloes Vej 5, Copenhagen DK-2200, Denmark. e-mail: morten.frodin@bric.ku.dk.

Acknowledgments
The authors would like to thank Britt Christoffersen, the HistoCore facility, Finsen Laboratory/BRIC, for excellent support with histology; Olga Ostrup, Center for Genomic Medicine, Rigshospitalet, University of Copenhagen, for help with whole-exome sequencing data; and Klaus Quortrup and Bente Stricker, Core Facility for Integrated Microscopy, University of Copenhagen, for electron microscopy.

Conflicts of interest
The authors disclose no conflicts.

Funding
This work was supported by the Danish Cancer Society (R146-A9563-B3551 to F.N. and R124-A7632-15-S2 to M.F.), the Danish Council for Independent Research (DFF-Mobilex 4092-00235 to F.N. and 0602-02368B to M.F.), the Lundbeck Foundation (R165-2013-15743 to F.N.), the University of Copenhagen Excellence Programme for Interdisciplinary Research—CDO2016 (to M.F.) and NIH R01 CA205158, R21 CA184656 and an endowed investigatorship from the Roy and Lynne Frank Foundation (to S.H.H.).

Supplementary Materials and Methods

Animal Housing and Approvals

Mice were housed in Green line type II IVC plastic cages (Tecniplast, Buguggiate, VA, Italy) in a temperature-controlled pathogen-free animal facility, with unrestricted access to diet (Altromin #1324, Altromin, Lage, Germany) and tap water. The animal room had a 12:12 hour light-dark cycle (lights on at 06.00). Mice were given nesting material, shredded paper strips, and shelters as environmental enrichment. Bedding was aspen wood chips supplied by Tapvei (TAPVEI OÜ Tapvei, Estonia). The experiments were approved by the Danish Experimental Inspectorate (protocol approval #2013-15-2934-00986) and housing of the mice was carried out according to Danish legislation and the Directive 2010/63/EU on the protection of animals used for scientific purposes.

Estimation of the Efficiency of Engineering Dnajb1–Prkaca *In Vivo*

Livers were collected 3 days after hydrodynamic tail vein delivery of CRISPR/Cas9 plasmids and genomic DNA was extracted using QIAmp DNA Mini Kit (Qiagen) following manufacturer's instruction. We first confirmed the generation of the *Dnajb1–Prkaca* fusion by PCR amplification of the genomic breakpoint using HotStar Master Mix Kit (Qiagen) and *Dnajb1*–Fwd1 and *Prkaca*-Rev1 as primer pair. Next, we estimated the number of copies of the *Dnajb1–Prkaca* allele in the genomic DNA. To this end, we PCR amplified serial dilutions of a genomic DNA sample containing the *Dnajb1–Prkaca* fusion and quantified the intensity of each PCR amplicon run on a 2% agarose gel with ImageJ software (http://rsbweb.nih.gov/ij/). With these data we generated a calibration curve that was used to estimate the number of copies of *Dnajb1–Prkaca* by measuring the intensity of amplicons generated by PCR on genomic DNA from the liver of the hydrodynamically injected mice.

Transmission Electron Microscopy

Formalin-fixed and paraffin-embedded tumor and matched liver samples were de-paraffinized with xylene according to standard procedures and immersed in 2% v/v glutaraldehyde in 0.05 mol/L sodium phosphate buffer (pH 7.4) over night. Samples were rinsed 3 times in 0.15 mol/L sodium phosphate buffer (pH 7.4) and subsequently postfixed in 1% w/v OsO_4 and 0.05 mol/L potassium ferricyanide in 0.12 mol/L sodium phosphate buffer (pH 7.4) for 2 h. The specimens were dehydrated in graded series of ethanol, transferred to propylene oxide, and embedded in Epon according to standard procedures. Sections, approximately 80-nm thick, were cut with a Leica UC7 microtome and collected on copper grids with Formvar supporting membranes. Sections were stained with uranyl acetate and lead citrate and subsequently examined with a Philips CM 100 TEM (Philips, Eindhoven, The Netherlands), operated at an accelerating voltage of 80 kV. Digital images were recorded with an OSIS Veleta (Muenster, Germany) digital slow scan 2k × 2k CCD camera and the ITEM software package.

Genomic CRISPR/Cas9 Off-Target Analysis

Potential off-targets for the gRNA targeting *Dnajb1* intron 1 and for the gRNA targeting *Prkaca* intron 1 that were used in this study to generate the *Dnajb1–Prkaca* fusion were identified by using the online program http://crispor.tefor.net/crisporDev/crisporBeta/crispor.py. (Haeussler et al, Genome Biology, 2016;17:148) This program ranks potential off-target sites according to a score for probability of cutting. Nine predicted off-target sites for the Dnajb1 gRNA and 10 predicted sites for the Prkaca gRNA with the highest score were chosen for further analysis by IDAA. A list of the analyzed off-targets and PCR primers used for IDAA is given in Supplementary Table 1. IDAA was performed as described elsewhere in this manuscript on normal vs tumor-matched genomic DNA, with the normal DNA serving as a control. The amplified PCR fragments were run on an ABI 3500 genetic analyzer to identify possible indels in the off-target site of interest.

Genomic PCR of the Dnajb1–Prkaca Fusion on Laser Capture Microdissected Tumors

The genomic region encompassing the *Dnajb1–Prkaca* breakpoint was amplified by a 2-step nested PCR using the primer pairs *Dnajb1*–Fwd1/*Prkaca*–Rev1 in the first step and *Dnajb1*–Fwd2/*Prkaca*–Rev2 in the second step. The non-edited *Prkaca* region was co-amplified using the primers *Prkaca*–Fwd3/*Prkaca*–Rev3 in both steps. The template in step 2 was 1 μL of the step 1 PCR. The cycle conditions of step 1 were: initial denaturation for 15 min at 95°C, then 15 touchdown cycles of denaturation for 30 s at 95°C, annealing for 30 s at 72°C (with a decrease in temperature by 1°C in each cycle) and extension for 30 s at 72°C, then 15 cycles with same conditions except that the annealing temperature was constant at 58°C followed by a final extension step for 5 min at 72°C. In step 2, identical cycle conditions were used, except for 25 cycles in the amplification step. PCR was performed in 25 μL with final concentrations/amounts of reagents as follows: 1.2 U TEMPase Hot Start DNA polymerase (Ampliqon, Odense, Denmark), 1x ammonium buffer with 2.5 mmol/L $MgCl_2$ (Ampliqon), 1 mmol/L dNTP (Ampliqon), and 0.25 μmol/L of each primer. Amplification of PCR products of the proper size was verified by agarose gel electrophoresis. Finally, fusion PCR products were cloned and Sanger sequenced to determine the sequence.

mRNA Expression Profiling

Freshly dissected tumor or normal liver tissues from control-injected mice were snap-frozen in liquid nitrogen. Total RNA was extracted from the tissue using QIAshredder spin columns (Qiagen) and RNeasy Mini Kits (Qiagen) and RNA integrity number was determined in an Agilent Technologies 2100 Bioanalyzer using the Agilent RNA 6000 Nano

kit (Agilent Technologies, Glostrup, Denmark). Libraries for RNA sequencing were prepared using the NEBNext Ultra Directional RNA Library Prep Kit for Illumina (NEB #E7420) and NEBNext rRNA Depletion Kit (NEB #E6310), according to the manufacturer's instructions (New England Biolabs, Ipswich, MA). Library quality was assessed in an Agilent Technologies 2100 Bioanalyzer using the Agilent DNA 1000 kit (Agilent Technologies), quantified using the Qubit dsDNA HS assay kit (Thermo Fisher Scientific) and diluted before sequencing on an Illumina NextSeq 500 sequencing platform. The raw data was converted from bcl to fastq format and the samples demultiplexed using the Illumina command line tool bcl2fastq v2.18.0.12.

Raw reads in fastq format were quality assessed with FastQC[1] and Fastq Screen[2] and afterwards trimmed using Trimmomatic v0.32[3] (non-default settings: -phred33 HEADCROP:12 LEADING:3 TRAILING:3 SLIDINGWINDOW:4:15 MINLEN:25). The trimmed reads were aligned to the mouse (mm10 assembly) genome with the STAR alignment tool v2.5.1a[4] (non-default settings: –readFilesCommand zcat –sjdbGTFfile <GTF> –sjdbOverhang 63 –twopassMode Basic –outSAMtype BAM SortedByCoordinate –outSAMattributes All –outSAMunmapped Within –outFilterMismatchNoverLmax 0.1 –outFilterMatchNmin 16 –outFilterMismatchNmax 5). Uniquely mapped reads were assigned to RefSeq database genes (gtf format, downloaded from University of California Santa Cruz with date stamp Oct 2nd 2016) with featureCounts v1.5.1[5] (none-default settings: -T 10 -s 2 -J –donotsort). Both genome and gene annotation was limited to the canonical genome sequences. The raw gene counts were imported into the statistical software R (v3.3.1),[6] counts from technical replicates merged and further processed and analyzed using the DESeq2 R-package (v1.14.1).[7] Because no biological replicates were available, no statistical tests were performed, but based on normalized and variance-stabilized counts ('rlogTransformation'), a simple log2 fold change was calculated.

The Sashimi plot was constructed with the Miso package (v0.5.3)[8] and is based on 1 normal liver and the FL-HCC sample alignment files. In addition, we compared our expression data to previously published studies, either through GSEA for human FL-HCC data (Cornella et al,[9] Simon et al,[10] Xu et al[11]) or through direct comparison with mouse tissue expression data (Lee et al[12]). We chose to compare with the human data using only gene lists of differentially expressed genes to bypass direct meta-analyses cross-organism and cross-platform. Because the Cornella et al study did not include expression results from a comparison of normal and FL-HCC samples, we downloaded the raw (except for background subtraction) expression microarray data (GSE57725) and reanalyzed it for our purpose. We variance-stabilized (vsn), log transformed, and finally quantile normalized the background-corrected data. Based on the sample annotation of *Dnajb1–Prkaca* fusion (Present/Absent/NA) in the Cornella et al publication Figure 5, we excluded tumor samples where the fusion was not demonstrated and excluded further 5 samples because of uneven quality. We performed a standard statistical analysis on the normalized data using the limma package (v3.30.13)[13] for FL-HCC (N=23) vs normal (N=3) and called differentially expressed genes with FDR<=5%. GSEA GseaPreranked (command-line tool v3.0) was run with default settings on our results of genes ranked by log2 fold change (or absolute log2 fold change). Our ranked genes were compared with either gene sets downloaded from the MSigDB[14] (v6) (nperm=1000) or to the specific FL-HCC vs Normal gene sets from Simon et al, 2015 (Data Set 1,STRICT: abs(log2fc)>=3,baseMean>=25), Xu et al, 2015 (Supplementary Table 3) and Cornella et al, 2015 (FDR<=5%) (Supplementary Figure 5*A*) (nperm=10000). For Figure 4*B*, we considered differentially regulated genes as those genes with absolute log2 fold change higher than 1.5 and average normalized count ('baseMean') above 25. Gene Ontology analysis on directionally concordant differentially regulated genes was performed using the Molecular Signature Database (MSigDB) v6.0 from Broad Institute (http://software.broadinstitute.org/gsea/msigdb).[14]

Raw transcriptomic paired-end mouse data published[12] was downloaded from Gene Expression Omnibus (GSE71873). To make the data as comparable with our data as possible, the downloaded sequencing data was treated as single-end reads and trimmed to the same length, but otherwise processed identically to our own data (except s=0 for featureCounts). After combining gene counts of the 2 datasets in R and normalizing for sequencing depth ('betweenLaneNormalization','method=full') with the EDASeq package (v2.6.2)[15] we removed visible batch effect (estimated from PCA plots) with the RUVg function (k=1,drop=0) from the RUVSeq package (v1.6.2).[16] The heatmap cells contain the Spearman correlation coefficients for all pairwise sample comparisons. The symmetric row and column dendrograms based on these correlations were calculated using Euclidian distance and the 'complete' clustering method.

Whole-Exome Sequencing and SNV Validation

DNA for whole-exome sequencing was either isolated from freshly frozen tissue or from formalin-fixed paraffin-embedded tumor samples. Each pair of normal and tumor sample was derived from the same animal and the DNA was isolated from tissue that had undergone the same fixation and storage procedure. Exome capture using SureSelectXT Mouse All Exon Kit (Agilent Technologies) and sequencing at a depth of $>27x10^6$ reads per sample to obtain sufficient coverage for mutation analysis on the Illumina NextSeq 500 sequencer were performed by GenomeScan (www.genomescan.nl). A pipeline based on the Genome Analysis Toolkit (GATK) Best Practices (https://software.broadinstitute.org/gatk/) recommendations was used throughout the analysis. Reads were trimmed, filtered, and mapped using Burrows-Wheeler Alignment (BWA v0.7.4-default mismatch rate of 4%) to reference assembly (ucsc.mm9.fasta). The MuTect algorithm v1.1.4[17] was used to identify somatic variants that differed between normal and tumor DNA, and the MuTect2 algorithm was used to identify indels. Finally, all tumor-specific SNVs

and indels were inspected and confirmed using Integrative Genomics Viewer v2.3 software from the Broad Institute (Boston) (https://software.broadinstitute.org/software/igv/). Sanger sequencing was used to validate select SNVs and IDAA to validate the indel. Primers are listed in Supplementary Table 1.

Genomic PCR of Cancer Genes on Laser Capture Microdissected Tumors

Five microdissected and *Dnajb1–Prkaca*-positive tumors were analyzed by PCR and Sanger sequencing for the presence of mutations in known hotspots of human liver cancer genes (*Kras*-G12, *Ctnnb1*-Exon3, *Trp53*-R172, *Trp53*-R248, *Trp53*-R270) or for a gene found frequently mutated in mouse models of hepatocellular carcinoma (*Hras-Q61*). Primers are listed in Supplementary Table 1.

Immunoblotting

Freshly dissected tumor or adjacent normal liver tissue was snap-frozen in liquid nitrogen, then lysed in RIPA buffer supplemented with protease and phosphatase inhibitors and normalized for protein content using BCA protein assay (Thermo Fisher Scientific). Proteins were fractionated by SDS-PAGE, blotted onto nitrocellulose membrane using standard techniques, and subjected to immunoblotting using rabbit anti-PKA Cα antibody (sc-903, Santa Cruz Biotechnology), rabbit anti-Aurora A antibody (#A300-072A, Bethyl Laboratories, Inc, Montgomery, TX) or mouse anti-Vinculin antibody (#V9131, Sigma). Primary antibodies were visualized using horseradish peroxidase-coupled anti-rabbit/mouse antibodies and SuperSignal West Femto Maximum Sensitivity enhanced chemiluminescence substrate (Thermo Fisher Scientific).

References

1. Andrews S. http://www.bioinformatics.babraham.ac.uk/projects/fastqc.
2. Andrews S. http://www.bioinformatics.babraham.ac.uk/projects/fastq_screen/.
3. Bolger AM, Loshe M, Usadel B. Trimmomatic: a flexible trimmer for Illumina sequence data. Bioinformatics 2014;30:2114–2120.
4. Dobin A, Gingeras TR. Mapping RNA-seq Reads With STAR. Bioinformatics 2013;29:15–21.
5. Liao Y, Smyth GK, Shi W. featureCounts: an efficient general purpose program for assigning sequence reads to genomic features. Bioinformatics 2014;30:923–930.
6. R Core Team. https://www.R-project.org/.
7. Love MI, Huber W, Anders S. Moderated estimation of fold change and dispersion for RNA-seq data with DESeq2. Genome Biol 2014;15:550.
8. **Wang ET, Sandberg R**, Luo S, et al. Alternative isoform regulation in human tissue transcriptomes. Nature 2008;456:470–476.
9. Cornella H, Alsinet C, Sayols S, et al. Unique genomic profile of fibrolamellar hepatocellular carcinoma. Gastroenterology 2015;148:806–818.e10.
10. Simon EP, Freije CA, Farber BA, et al. Transcriptomic characterization of fibrolamellar hepatocellular carcinoma. Proc Natl Acad Sci U S A 2015;112:E5916–E5925.
11. Xu L, Hazard FK, Zmoos AF, et al. Genomic analysis of fibrolamellar hepatocellular carcinoma. Hum Mol Genet 2015;24:50–63.
12. Lee DH, Park JO, Kim TS, et al. LATS-YAP/TAZ controls lineage specification by regulating TGFβ signaling and Hnf4α expression during liver development. Nat Commun 2016;7:11961.
13. Ritchie ME, Phipson B, Wu D, et al. limma powers differential expression analyses for RNA-sequencing and microarray studies. Nucleic Acids Res 2015;43:e47.
14. **Subramanian A, Tamayo P**, Mootha VK, et al. Gene set enrichment analysis: a knowledge-based approach for interpreting genome-wide expression profiles. Proc Natl Acad Sci U S A 2005;102:15545–15550.
15. Risso D, Schwartz K, Sherlock G, et al. GC-Content Normalization for RNA-Seq Data. BMC Bioinformatics 2011;12:480.
16. Risso D, Ngai J, Speed TP, et al. Normalization of RNA-seq data using factor analysis of control genes or samples. Nat Biotechnol 2014;32:896–902.
17. Cibulskis K, Lawrence MS, Carter SL, et al. Sensitive detection of somatic point mutations in impure and heterogeneous cancer samples. Nat Biotechnol 2013;31:213–219.

Author names in bold designate shared co-first authorship.

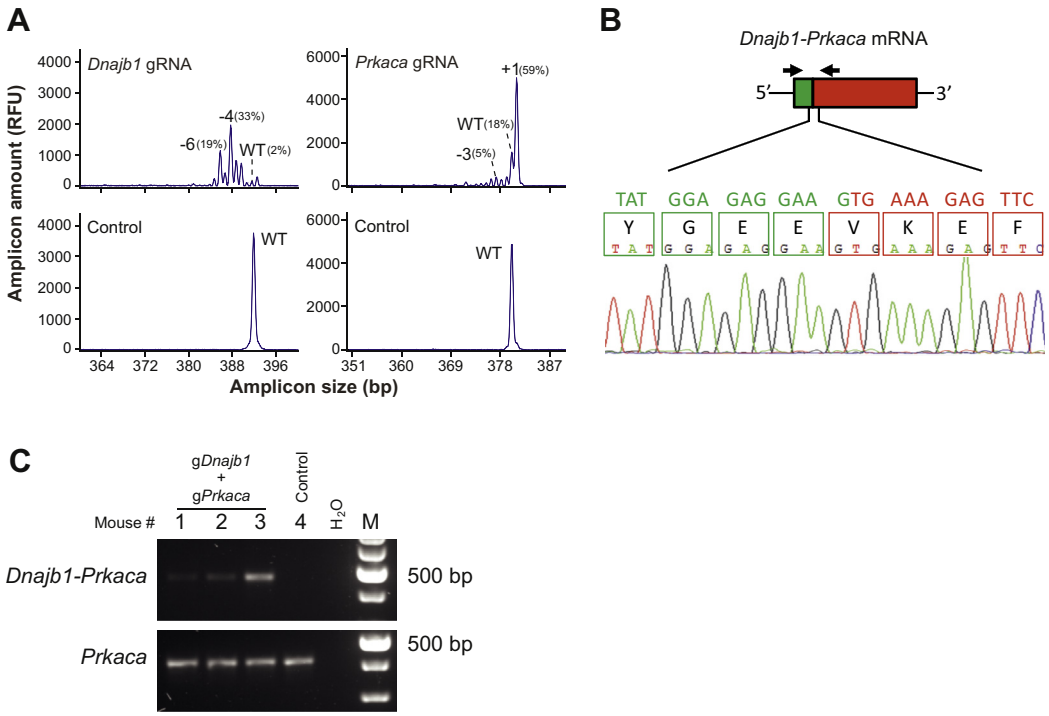

Supplementary Figure 1. Testing of CRISPR/Cas9 reagents for engineering of the *Dnajb1–Prkaca* fusion. (*A*) Efficiency of the gRNAs shown in Figure 1*A* to introduce a DNA double-strand break in intron 1 of *Dnajb1* or intron 1 of *Prkaca*, as assessed by IDAA on a pool of Neuro-2a cells transfected with the gRNAs. IDAA profiles show amplicons generated for wild-type (WT) and indel mutation alleles, with indication of indel size and frequency for select amplicons. For comparison, IDAA profiles for non-edited Neuro-2a cells are shown, which contain the WT amplicon only (control). (*B*) *Dnajb1–Prkaca* mRNA specific PCR on cDNA generated from Neuro-2a cells transfected with the *Dnajb1/Prkaca* gRNA pair shown in Figure 1*A* demonstrates the expression of an in-frame fusion transcript (Sanger sequencing chromatogram). Schematic of the fusion transcript shows the location of primers (*arrows*) used to amplify the fusion breakpoint. (*C*) Efficiency of the gRNA pair shown in Figure 1*A* to elicit the *Dnajb1–Prkaca* fusion in the liver of hydrodynamically tail vein injected mice. *Dnajb1–Prkaca* specific PCR from DNA isolated from livers 3 days post injection is shown. PCR for *Prkaca* in a non-edited region is shown as an internal PCR control.

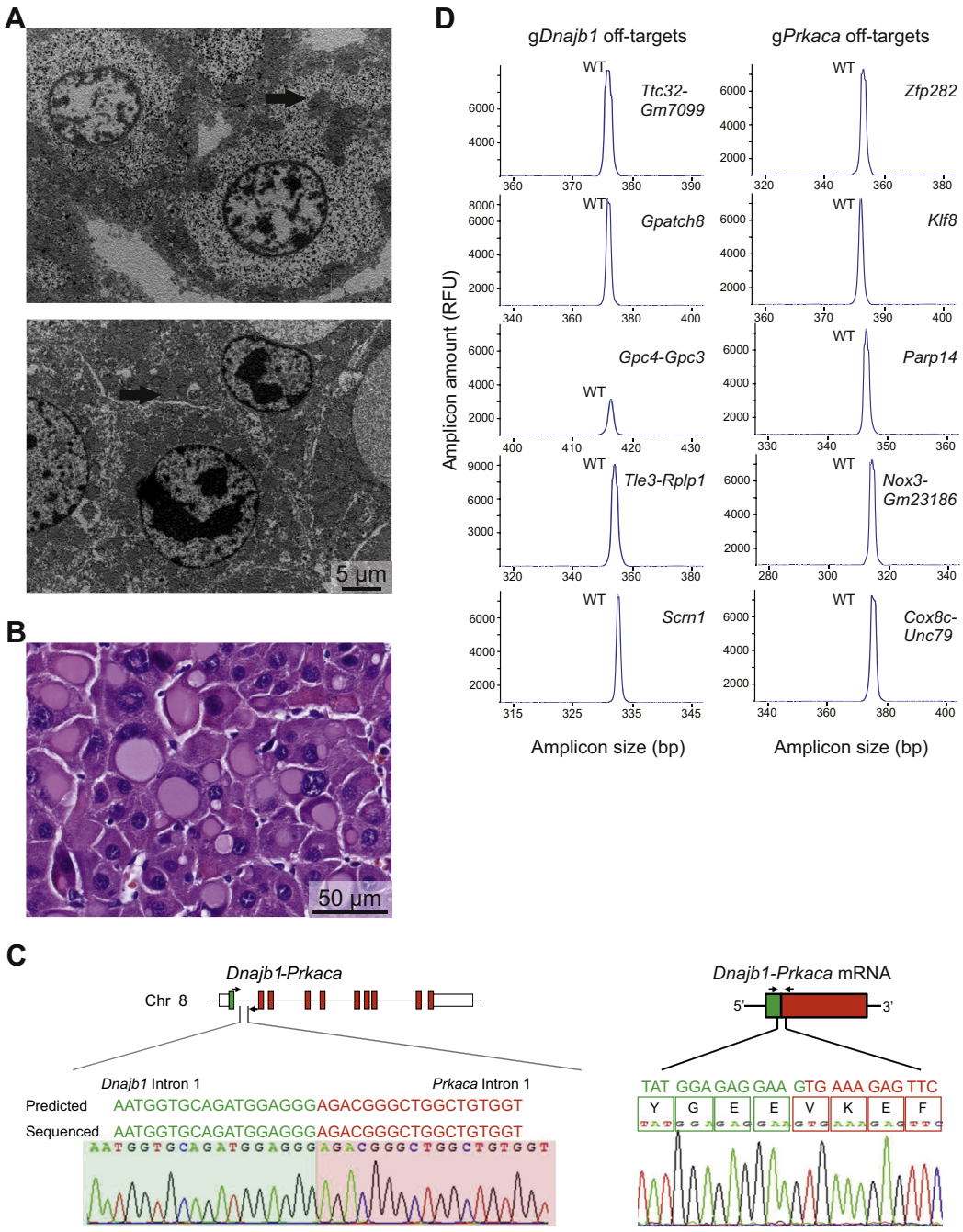

Supplementary Figure 2. The *Dnajb1–Prkaca* fusion elicits FL-HCC in mice. (*A*) Transmission electron micrograph showing tumor cells with abundant mitochondria (*arrows*) in the cytoplasm and nuclei with prominent nucleoli (*bottom panel*), as compared with more sparse mitochondria in hepatocytes of the non-tumorous part of the liver (*top panel*). (*B*) Microscopic H&E image of FL-HCC tumor area with many tumor cells showing "pale bodies", hyaline globules and features of oncocytic hepatocytes. (*C*) DNA (*left*) and RNA (*right*) Sanger sequence chromatograms of the *Dnajb1–Prkaca* fusion derived from the tumor in Figure 2*A*. Genomic and reading frame breakpoints are shown. *Arrows* indicate location of primers used for PCR amplification. (*D*) No evidence is detected of off-target cutting induced by the gRNA pair in the tumor shown in Figure 2*A*, as IDAA shows only a wild-type peak at the top-ranking, predicted off-target sites for each gRNA.

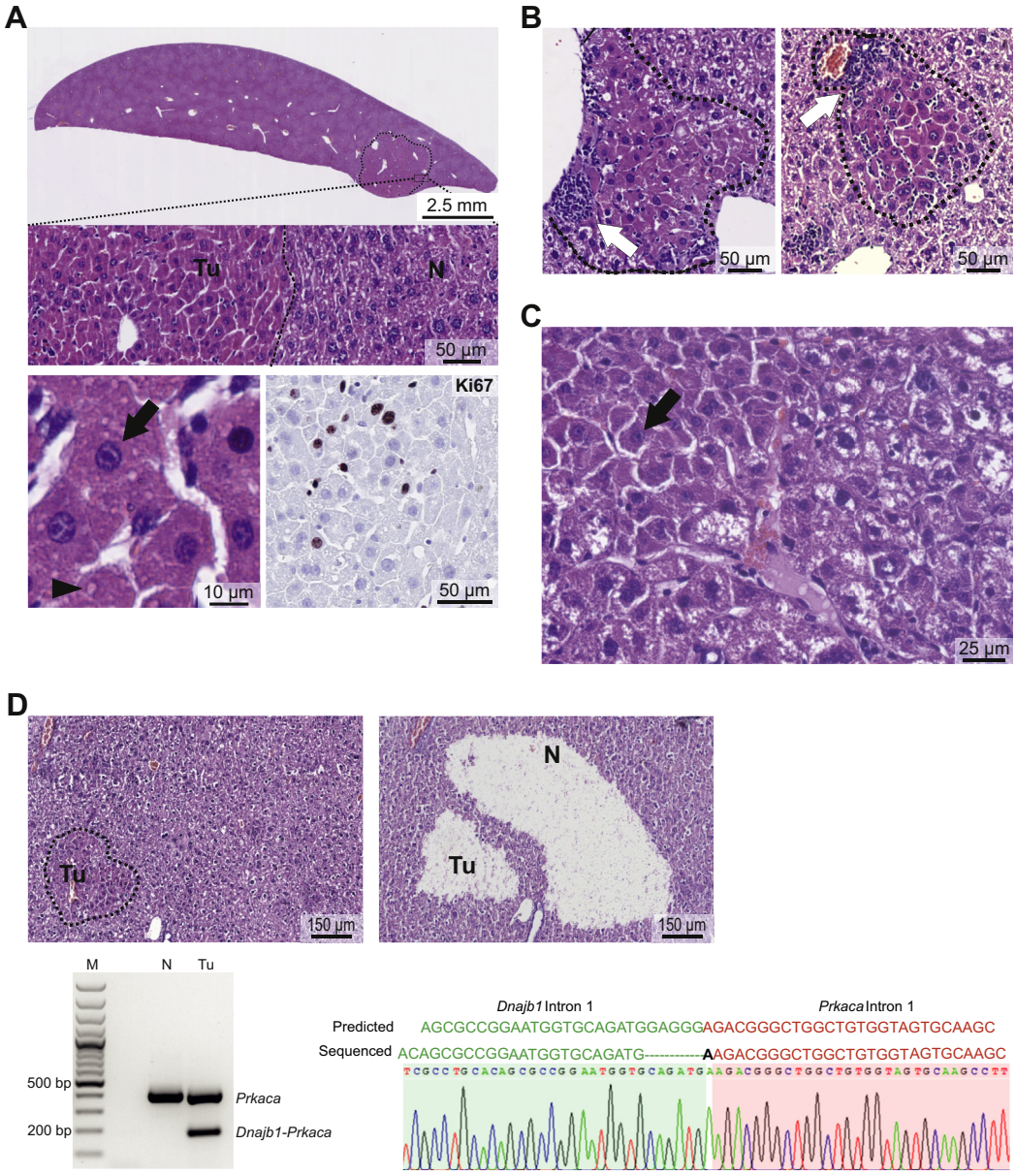

Supplementary Figure 3. Various examples of *Dnajb1–Prkaca* fusion induced tumors (*A*) Exposed tumor demarcated from the surrounding non-tumorous liver tissue by pushing margin (*upper panel*) and appearing with eosinophilic, granular "oncocytic" cells in tumor area (Tu), as compared with the normal hepatocytes of the non-tumorous area (N) (*middle panel*). The bottom left panel shows details of "oncocytic" granular hepatocyte-like cells containing nuclei with prominent nucleoli (*arrow*), "pale bodies" and hyaline globules (*arrowhead*). Ki67-staining shows that tumor cells are proliferating (*bottom right panel*). (*B*) Examples of small neoplastic lesions with large "oncocytic" granular hepatocyte-like cells and leukocyte infiltration (*white arrows*). (*C*) Mixed-FL-HCC. Lesion showing cells with features of oncocytic hepatocytes (*black arrow*) and cells with a clear-cell phenotype. (*D*) Demonstration of the *Dnajb1–Prkaca* fusion in small neoplastic lesions by laser capture microdissection and genomic PCR. A small lesion (Tu) to be analyzed (*upper left*). Microdissection of the lesion (Tu) and adjacent non-tumorous tissue (N) performed on the neighboring section, which is shown after capture of the tissue (*upper right*). Genomic PCR on captured tissue showing amplification of the *Dnajb1–Prkaca* fusion from the lesion (Tu), but not from the normal liver tissue (N), whereas a region in *Prkaca* not affected by the editing is amplified from both samples, serving as an internal PCR control (*bottom left*). Sanger sequencing chromatogram for the fusion breakpoint of cloned *Dnajb1–Prkaca* amplicon from this tumor is shown as an example (*bottom right*).

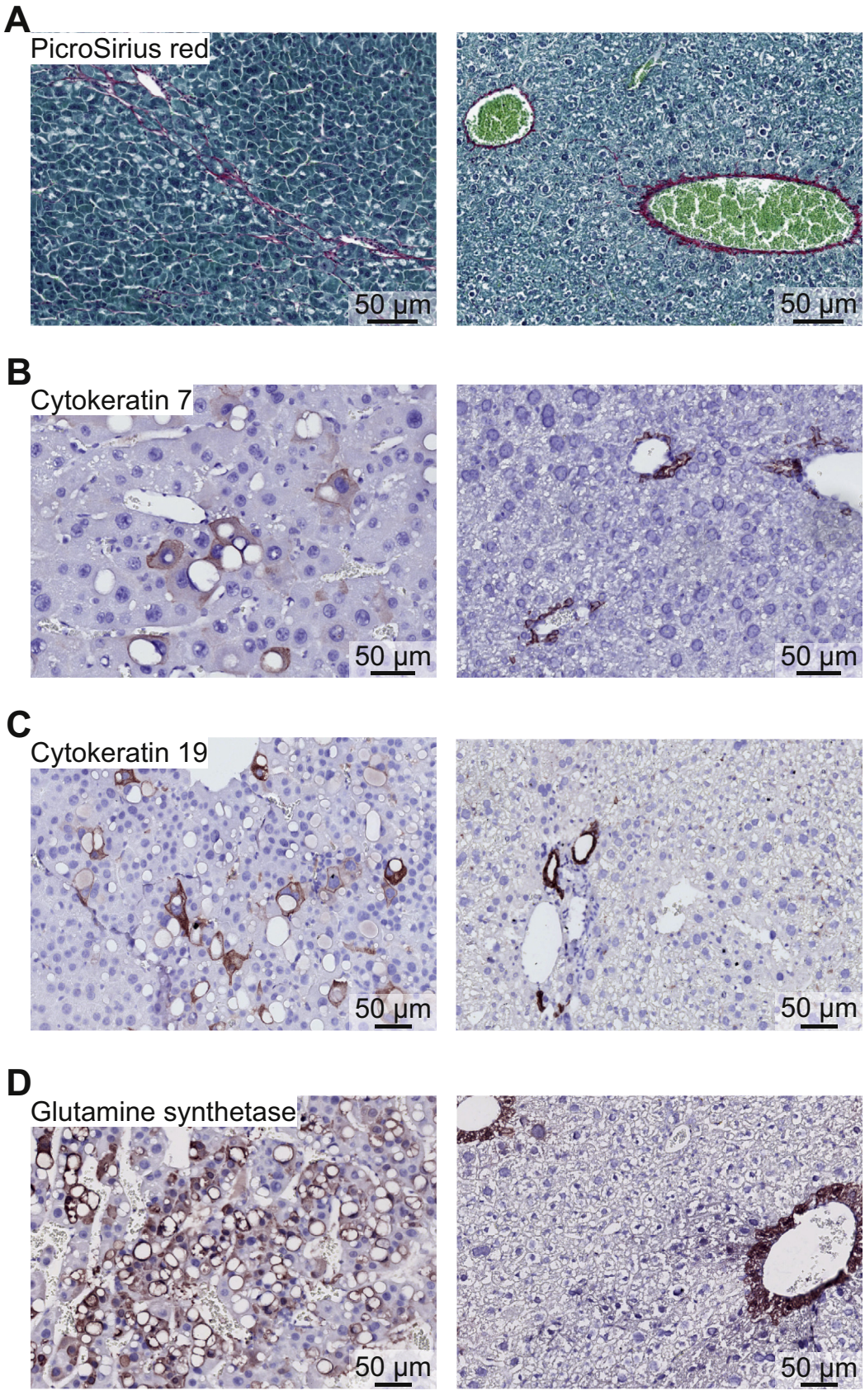
A
PicroSirius red
50 μm
50 μm
B
Cytokeratin 7
50 μm
50 μm
C
Cytokeratin 19
50 μm
50 μm
D
Glutamine synthetase
50 μm
50 μm

Supplementary Figure 4. Histologic characterization of the *Dnajb1–Prkaca*-induced mouse FL-HCC. (*A*) PicroSirius red staining showing mild collagen fibrosis (red) between cells in tumor area (*left*), whereas in the adjacent normal liver area collagen is confined to blood vessels (*right*). (*B*) Cytokeratin 7 staining showing scattered expression in tumor cells (*left*), but only expression in bile ducts in the normal part of the same liver. (*C*) Cytokeratin 19 expression in tumor cells (*left*), whereas in the normal part of the liver, only bile ductal cells and hepatic progenitor cells are positive (*right*). (*D*) Glutamine synthetase expression in tumor (*left*) and in hepatocytes adjacent to the central vein in normal liver (*right*).

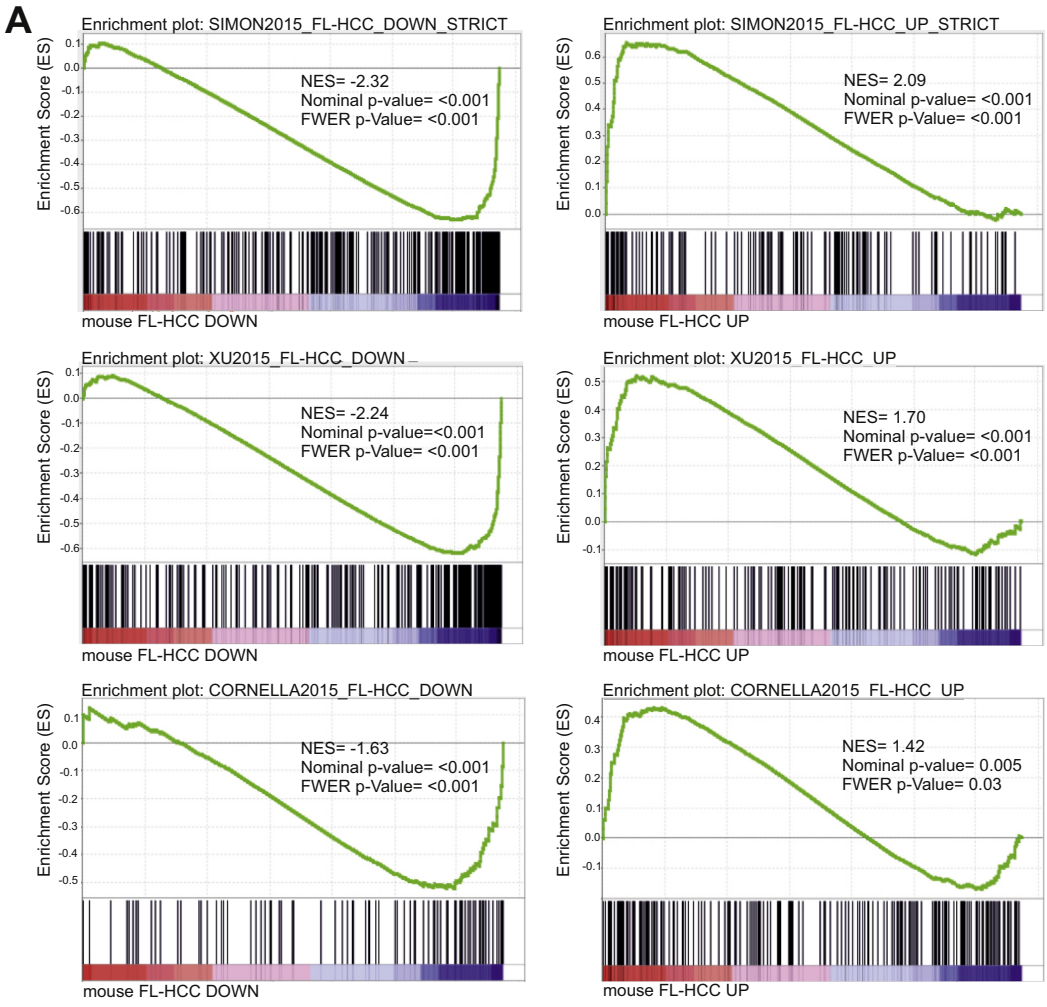
A
Enrichment plot: SIMON2015_FL-HCC_DOWN_STRICT
NES= -2.32
Nominal p-value= <0.001
FWER p-Value= <0.001
mouse FL-HCC DOWN
Enrichment plot: SIMON2015_FL-HCC_UP_STRICT
NES= 2.09
Nominal p-value= <0.001
FWER p-Value= <0.001
mouse FL-HCC UP
Enrichment plot: XU2015_FL-HCC_DOWN
NES= -2.24
Nominal p-value=<0.001
FWER p-Value= <0.001
mouse FL-HCC DOWN
Enrichment plot: XU2015_FL-HCC_UP
NES= 1.70
Nominal p-value= <0.001
FWER p-Value= <0.001
mouse FL-HCC UP
Enrichment plot: CORNELLA2015_FL-HCC_DOWN
NES= -1.63
Nominal p-value= <0.001
FWER p-Value= <0.001
mouse FL-HCC DOWN
Enrichment plot: CORNELLA2015_FL-HCC_UP
NES= 1.42
Nominal p-value= 0.005
FWER p-Value= 0.03
mouse FL-HCC UP
Enrichment Score (ES)

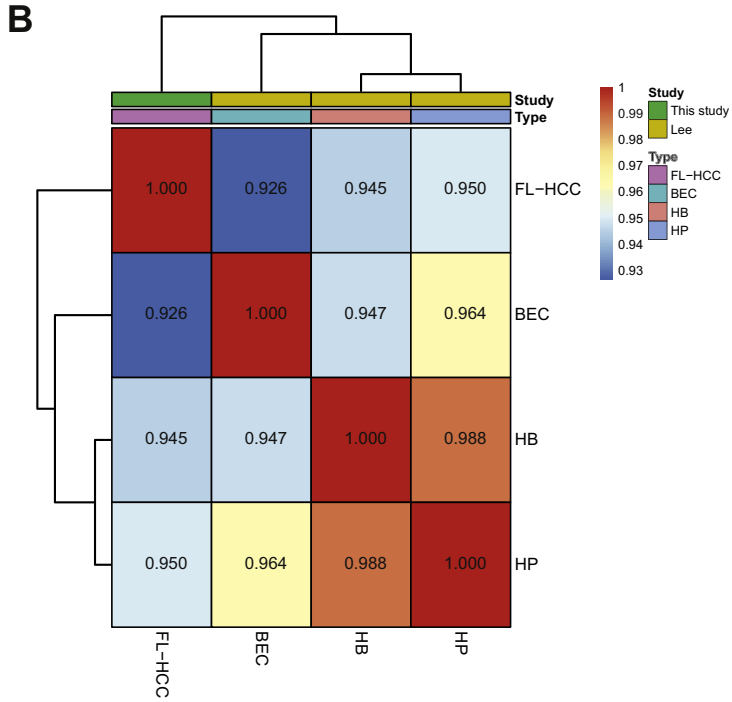
B
Study
Type
1.000
0.926
0.945
0.950
FL−HCC
0.926
1.000
0.947
0.964
BEC
0.945
0.947
1.000
0.988
HB
0.950
0.964
0.988
1.000
HP
FL−HCC
BEC
HB
HP
1
0.99
0.98
0.97
0.96
0.95
0.94
0.93
Study
This study
Lee
Type
FL−HCC
BEC
HB
HP

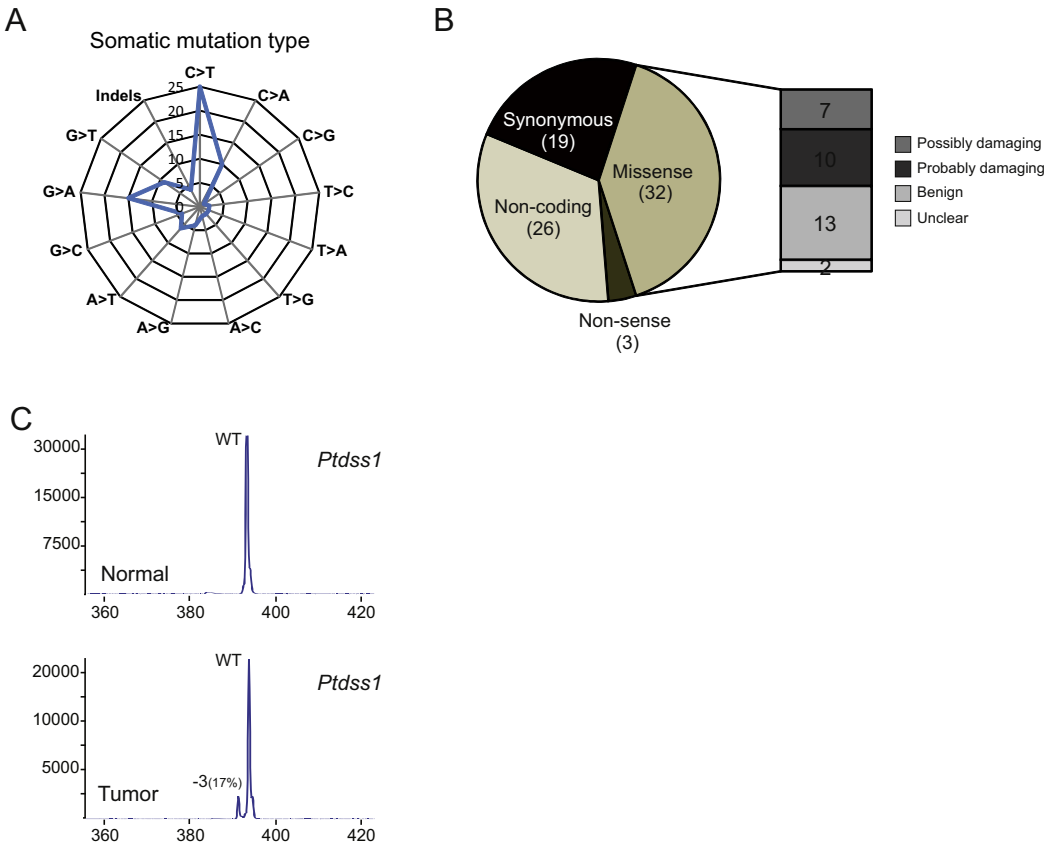

Supplementary Figure 6. Somatic mutations in mouse FL-HCC driven by *Dnajb1–Prkaca.* (*A*) Graphical representation of the type of somatic mutations identified by whole-exome sequencing in a larger mouse FL-HCC tumor. Counts for each type of base substitutions and for indels are indicated. (*B*) Pie chart depicting the distribution of the somatic mutations as Non-coding, Synonymous, Non-sense, and Missense. The Missense mutations were classified as Possibly damaging, Probably damaging and Benign, according to PolyPhen2 algorithm. Unclear: no damaging score available. (*C*) Validation by IDAA of the 3 basepair deletion in the non-coding region of *Ptdss1* from the larger mouse FL-HCC tumor. IDAA profile of *Ptdss1* from normal and tumor tissue is shown. WT: wild-type peak derived from unedited allele from normal and FL-HCC tissue. The frequency of the indel-mutated allele in the tumor is shown.

Supplementary Figure 5. Molecular characterization of *Dnajb1–Prkaca*-induced mouse FL-HCC. (*A*) GSEA showing negative (*left*) and positive (*right*) enrichment plots of mouse FL-HCC in comparison with human FL-HCC transcriptomic data. For each plot, NES (Normalized enrichment score), Nominal *P* value and FWER adjusted *P* value are indicated. SIMON2015_FL-HCC_DOWN/UP_STRICT, XU2015_FL-HCC_DOWN/UP and CORNELLA2015_FL-HCC_DOWN/UP refer to gene sets containing exclusively down- or up-regulated genes in references 29, 8 and 11. (*B*) Heat-map showing clustering of mouse FL-HCC transcriptome with mouse biliary epithelial cells (BEC), Hepatoblasts (HB), and Hepatocytes (HP) RNA-seq data as reported by reference 31.